CAVITY RESONATORS AND WAVE GUIDES CONTAINING PERIODIC ELEMENTS

By

HERBERT GOLDSTEIN

B.S., College of the City of New York

1940

SUBMITTED IN PARTIAL FULFILLMENT OF THE

REQUIREMENTS FOR THE DEGREE OF

DOCTOR OF PHILOSOPHY

FROM THE

MASSACHUSETTS INSTITUTE OF TECHNOLOGY

1943

Signature of Author

Department of Physics, May 10, 1943

Signature of Professor
Charge of Research .....

Signature of Chairman of Department
Committee on Graduate Students .....

TABLE OF CONTENTS

ACKNOWLEDGMENT

I wish to express my sincere gratitude to Professor J. C. Slater for having made this thesis possible, and for his continued interest and encouragement. To the members of the Theoretical Group, especially Professors H. A. Bethe and N. H. Frank, I am indebted for many suggestions and much helpful advice. Professor G. G. Harvey and Doctors H. Krutter and T. E. Lashof kindly supplied the experimental data for the corrugated wave guides and coaxial lines. I also wish to thank Professor A. E. Heins and the Staff of the Computing Room under his supervision for their wholehearted cooperation and aid.

ABSTRACT

I Resonant Modes of the Vane Magnetron

The resonant modes of vane type magnetrons are calculated, neglecting end effects and fringing near the vane edges. The effect of the cathode is considered and found to be negligible for all except the lowest modes. Tables are presented which facilitate the computation of the resonant wave lengths over a wide range of magnetron dimensions. The measured and computed values for three typical magnetrons differ by about 3%, presumably due to end effects. It is shown in Section II that the fringing of the fields could not account for more than a 1% difference.

II Effect of End Zones

Several methods of calculating the end zone effect in a linear magnetron are presented. In the first procedures appropriate tangential electric and magnetic fields in the end zones are joined to the corresponding fields in the oscillator cavities. These methods fail because the fields in the end zones and the fields in the cavity which corresponds to the region between the cathode and anode are not adequately matched. To improve this connection the currents on the walls of this region are joined continuously to the currents in the end zone walls. The calculated end zone effect is then in qualitative agreement with experiment. The remaining discrepancy is probably due to the omission of damped modes which are important near the edges of the vanes.

III Experimental Study of a Linear Magnetron

To investigate experimentally the effect of the end zones a 10 slot linear magnetron cavity with adjustable end plates has been constructed. Modes in the range from 6.5 to 12.5 cm. were detected and identified by means of the standing wave pattern picked up by a movable probe. The wave lengths of all the observed modes decrease as the end zone is reduced. However for the higher modes the decrease is slight, even at the smallest end zone used (.6 mm). Rough measurements of the unloaded Q were also made, and are approximately one half of the computed values.

IV The Corrugated Wave Guide

The linear magnetron used as a wave guide is known as a corrugated wave guide. Formulas are derived for the guide wave length and attenuation. The computed wave lengths are within 5% of the measured values, but the attenuation is about one fourth the actual value. It is shown that wave guides with relatively large end zones have the least attenuation.

V The Corrugated Coaxial Line

The corrugated coaxial line employs the same principle as the corrugated wave guide except that the slots are cut in the inner conductor. The wave length and attenuation in such a line are calculated both for empty slots and for slots filled with dielectric. Convenient approximate formulas for these quantities are presented which agree quite well with experiment. The attenuation due to losses in the dielectric is also considered.

CAVITY RESONATORS AND WAVE GUIDES

CONTAINING PERIODIC ELEMENTS

I. Resonant Modes of the Vane Magnetron

The resonant modes of slot and slot-and-hole magnetrons have been calculated by A. M. Clogston[1]. This section presents similar calculations for vane type magnetrons, i. e., in which the oscillator cavities are in the form of sectors of a cylinder.

An idealized type of vane magnetron will first be considered, a cross section of which is shown in Fig. 1. It is assumed long enough so that the end effects may be neglected. The cathode will also be omitted.

The space may be divided into two regions, the central cavity, I, and the individual oscillator cavities, II. In each region appropriate solutions of Maxwell's equations are used, obeying the boundary conditions on the metallic surfaces, which are considered ideal. Inside the oscillator cavities the radial component of the electric field will be neglected, that is, edge effects will not be taken into account.

The fields in each region are connected by requiring that the angular component of the electric field be continuous. The frequency at which the magnetron resonates is then determined by the condition that the axial component of the magnetic field vary continuously from Region I to II. Since the fields are only approximate, this condition cannot be fulfilled rigorously. One may however match the average magnetic field over the slot width.

---

[1] A. M. Clogston, Ph.D. Thesis, M.I.T., 1941

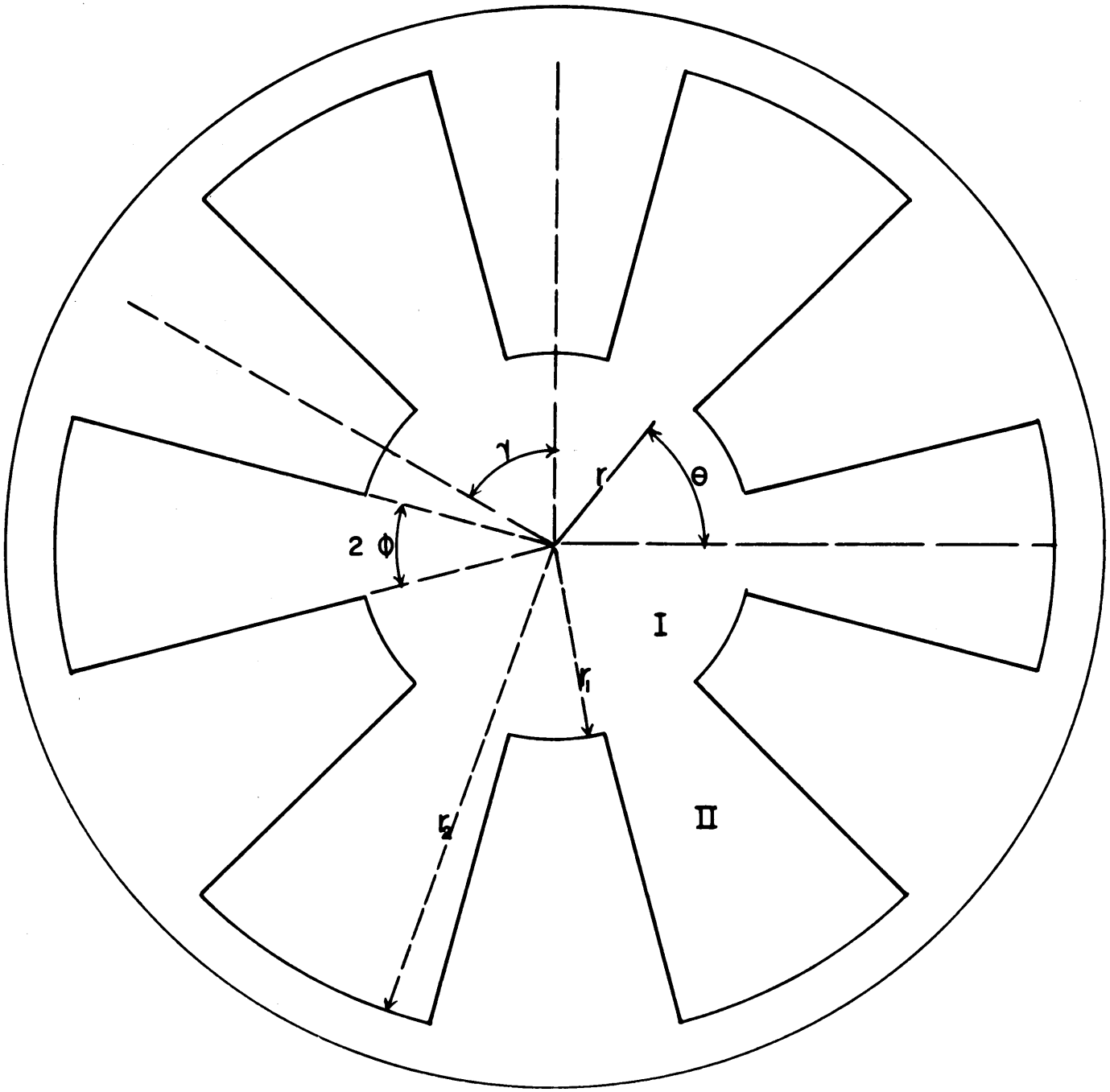

Fig. 1

M. I. T. RADIATION LAB. DWG. NO. X - 2385-A

In the jth oscillator the fields are:

$$\left.\begin{aligned} E_{\theta j} &= \frac{i\omega}{k} a e^{ijn\gamma'} \left[J_1(kr) N_1(kr_2) - N_1(kr) J_1(kr_2) \right] e^{-i\omega t}, \\ B_{zj} &= a e^{ijn\gamma'} \left[J_0(kr) N_1(kr_2) - N_0(kr) J_1(kr_2) \right] e^{-i\omega t}, \end{aligned}\right\} \quad (I-1)$$

$$k = \frac{\omega}{c} = \frac{2\pi}{\lambda}$$

where a is an arbitrary constant, n an integer, $\gamma' = \frac{2\pi}{N}$, N the number of oscillators. The phase factor $e^{ijn\gamma'}$ is necessary in order that the fields have the same periodicity as the oscillators. The time dependence $e^{-i\omega t}$ will be omitted in the following. The linear combinations of Bessel and Neumann functions used above are cylinder functions and will be designated by $C_1(k,r,r_2)$ and $C_{0,1}(k,r,r_2)$ where:

$$\left.\begin{aligned} C_m(k,r,r_2) &= J_m(kr) N_m(kr_2) - N_m(kr) J_m(kr_2) \\ C_{m,n}(k,r,r_2) &= J_m(kr) N_n(kr_2) - N_m(kr) J_n(kr_2) \end{aligned}\right\} \quad (I-2)$$

The fields may now be rewritten as:

$$\left.\begin{aligned} E_{\theta j} &= \frac{i\omega}{k} a e^{ijn\gamma'} C_1(k,r,r_2) \\ B_{zj} &= a e^{ijn\gamma'} C_{0,1}(k,r,r_2) \end{aligned}\right\} \quad (I-3)$$

In the central cavity, Region I, the appropriate solutions are standing waves. However traveling wave solutions may equally well be used, as the standing wave can always be obtained from the superposition of waves traveling in opposite directions. The fields to be used are:

$$\left.\begin{aligned} E_\theta &= -\sum_{m=-\infty}^{+\infty} \frac{i\omega}{k} b_m e^{im\theta} \frac{J_m'(kr)}{J_m'(kr_1)} \\ B_z &= -\sum_{-\infty}^{+\infty} b_m e^{im\theta} \frac{J_m(kr)}{J_m'(kr_1)} \end{aligned}\right\} \quad (I-4)$$

There is also an E_r component which is neglected.

The coefficients b_m are determined by the conditions on E_θ at the boundary between the two regions. There are, at $r = r_1$,

$$E_\theta(r_1) = E_{\theta j}(r_1), \qquad j\gamma - \phi < \theta < j\gamma + \phi$$
$$= 0 \qquad j\gamma + \phi < \theta < (j+1)\gamma - \phi$$
$$j = 0, 1, \cdots N-1.$$

where 2ϕ is the angular width of an oscillator cavity. The Fourier coefficients b_m turn out as follows:

$$b_m = -a \frac{C_1(R, r_1, r_2)\phi}{\pi} \frac{\sin m\phi}{m\phi} \sum_{j=0}^{N-1} e^{ij(n-m)\gamma} \qquad (I-5)$$

The geometric series in Eq. (I-5) vanishes except when $n - m = \pm \ell N$, $\ell = 0, 1, 2, \cdots$ when it is equal to N. The coefficients thus become

$$b_m = -a \frac{N\phi}{\pi} \frac{\sin m\phi}{m\phi} C_1(R, r_1, r_2), \qquad m = n \pm \ell N$$
$$= 0, \qquad \text{otherwise.} \qquad (I-6)$$

The average value of the magnetic field in I, averaged over the slot width of the jth oscillator cavity is:

$$\overline{B_z} = \sum b_m \frac{J_m(Rr_1)}{J_m'(Rr_1)} \frac{\sin m\phi}{m\phi} e^{ijm\gamma}$$
$$= -a \frac{N\phi}{\pi} C_1(R, r_1, r_2) \sum e^{ijn\gamma} \frac{J_m(Rr_1)}{J_m'(Rr_1)} \left(\frac{\sin m\phi}{m\phi}\right)^2 \qquad (I-7)$$

Equating this to the magnetic field in the oscillator cavity yields the following equation for the resonant frequencies:

$$\frac{N\phi}{\pi} \sum_{\substack{m = n \pm \ell N \\ \ell = 0, 1, 2, \cdots}} \frac{J_m(Rr_1)}{J_m'(Rr_1)} \left(\frac{\sin m\phi}{m\phi}\right)^2 = \frac{C_{0,1}(R, r_1, r_2)}{C_1(R, r_1, r_2)}. \qquad (I-8)$$

The left hand side of the equation is periodic in n with a period of N/2. Thus the terms for $n = n_1$ are the same as those for $n = n_1 + N/2$. Since n must be integral, the number of modes is limited to N/2 (or $\frac{N-1}{2}$ if N is odd).

Actual magnetrons differ in several points from the idealized type considered here. The vanes are not wedges, but are rectangular plates as shown in Fig. 2. The oscillator cavities may still be considered as very good approximations to sectors of a circle, but the center of the circle is now at O' instead of O. Then r_1 and r_2 in the oscillator fields are to be replaced by

$$r_1' = r_1 - \frac{d}{\tan \frac{r}{2}}$$
$$r_2' = r_2 - \frac{d}{\tan \frac{r}{2}} \qquad (I-9)$$

where 2d is the width of a vane. Eq. (I-8) becomes

$$\frac{N\phi}{\pi} \sum_{m=n\pm\ell N} \frac{J_m(kr_1)}{J_m'(kr_1)} \left(\frac{\sin m\phi}{m\phi}\right)^2 = - \frac{C_{0,1}(k, r_1', r_2')}{C_1(k, r_1', r_2)} \qquad (I-8')$$

If the cathode is included in the calculation, the fields in Region I become so modified that the tangential electric field vanishes over the cathode surface. The fields are then:

$$\left.\begin{aligned} E_\theta &= -\sum_{-\infty}^{+\infty} \frac{i\omega}{k} b_m e^{im\theta} \frac{J_m'(kr) N_m'(kr_3) - N_m'(kr) J_m'(kr_3)}{J_m'(kr_1) N_m'(kr_3) - N_m'(kr_1) J_m'(kr_3)} \\ B_z &= \sum_{-\infty}^{+\infty} b_m e^{im\theta} \frac{J_m(kr) N_m'(kr_3) - N_m(kr) J_m'(kr_3)}{J_m'(kr_1) N_m'(kr_3) - N_m'(kr_1) J_m'(kr_3)} \end{aligned}\right\} \qquad (I-10)$$

where r_3 is the radius of the cathode. The resonant frequencies are then

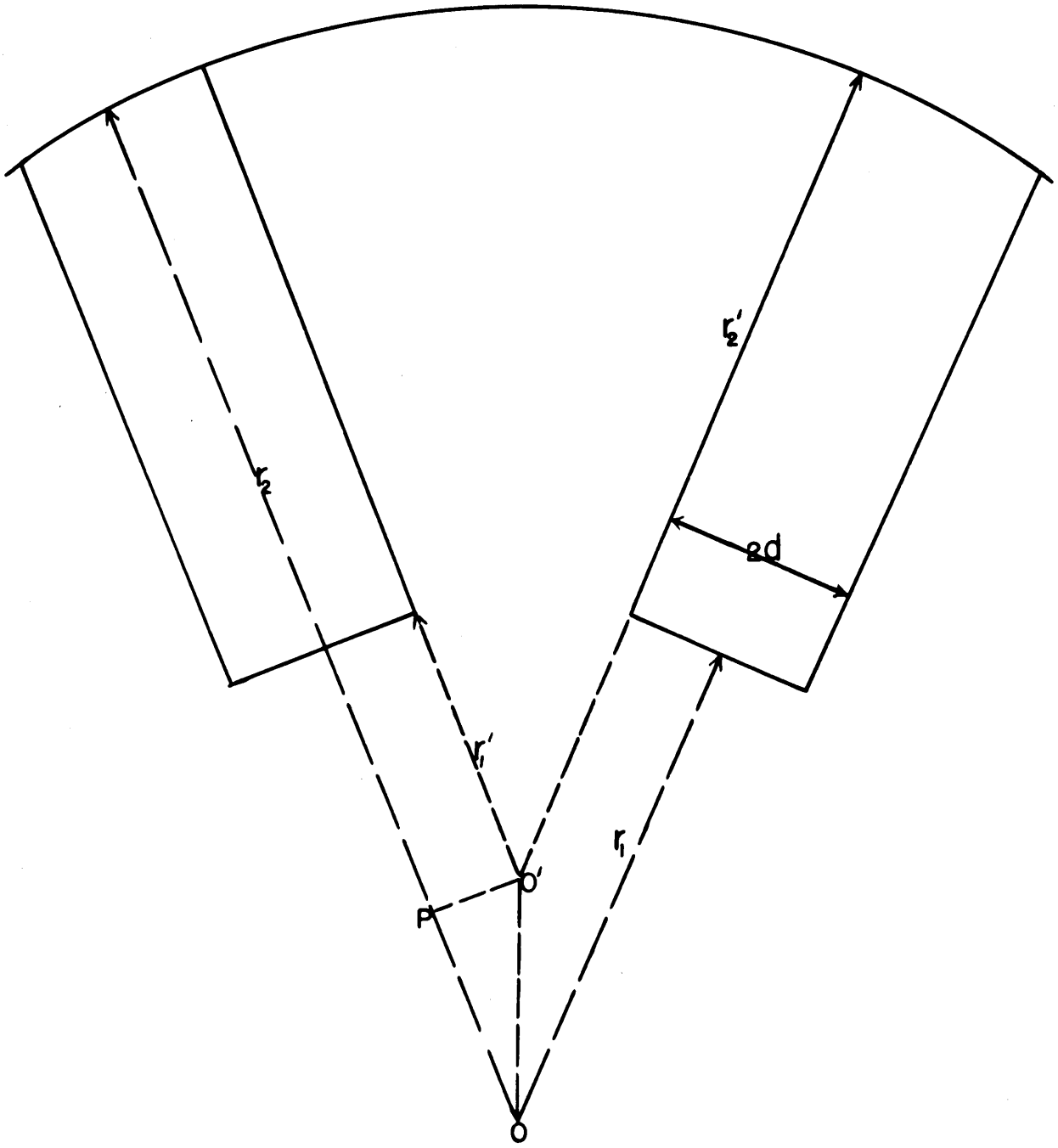

Fig. 2

roots of the following equation:

$$\frac{N\phi}{\pi} \sum_{m = n \pm \ell N} \frac{J_m(kr_1)\, N_m'(kr_3) - N_m(kr_1)\, J_m'(kr_3)}{J_m'(kr_1)\, N_m'(kr_3) - N_m'(kr_1)\, J_m'(kr_3)} \left(\frac{\sin m\phi}{m\phi}\right)^2 = - \frac{C_{o,1}(k, r_1', r_2')}{C_1(k, r_1', r_2')} \qquad (I-11)$$

When m is large, $J_m'(kr)$ is small except near the vanes and the introduction of the cathode will disturb the fields only slightly, and the resonant frequencies still less. Except for the lower modes the cathode has little effect, and therefore may be neglected in most cases.

For purposes of computation two functions f and G_n are defined by

$$f = \arctan\left(\frac{-C_{o,1}(k, r_1', r_2')}{C_1(k, r_1', r_2')}\right) \qquad (I-12)$$

and

$$G_n = \arctan\left(\sum_{m = n \pm \ell N} \frac{N\phi}{\pi} \frac{J_m(kr_1)}{J_m'(kr_1)} \left(\frac{\sin m\phi}{m\phi}\right)^2\right) \qquad (I-13)$$

The function f can be considered as a function of $x = k(r_2' - r_1') = k(r_2 - r_1)$ for different values of a parameter $y = r_2'/r_1'$. For the range of x encountered in most magnetrons f is very nearly a linear function,

$$f = a k (r_2 - r_1) + b \qquad (I-14)$$

Appendix I gives tables of a and b for various values of y. G_n considered as a function of kr_1 depends on the parameters N, n, and ϕ, and for n greater than 1 or 2 is quite accurately represented by a linear function

$$G_n = \alpha_n kr_1 + \beta_n \qquad (I-15)$$

for the ranges involved. When n is 1 or 2, the representation is not accurate, but may be used to give rough estimates. Tables of α_n and β_n are presented in Appendix I.

The resonant frequency is given by the root of

$$f = G_n$$

or in a convenient closed form:

$$R = \frac{b - \beta_n}{\alpha_n r_1 - a(r_2 - r_1)} \qquad (I-16)$$

The resonant wave lengths of three magnetrons have been calculated, neglecting the cathode, and are shown in Table I. For the first magnetron, which has a large cathode, the wave lengths have also been calculated including the cathode, using Eq. (I-11). The experimentally measured wave length, obtained from various sources, are also given in the table. Where two values are given for a mode, it indicates the mode was split into a doublet due to the loops and probes inserted in the magnetron. It is seen that the effect of the cathode in the first tube is negligible for the n = 4 and higher modes. The cathode must have an even smaller effect in the other tubes. In almost all cases the experimental wave length is lower than the theoretical value. For the second tube, the Westinghouse VA-1, part of this may be due to strap grooves near the extremity of the vanes. However the larger part of difference is the result of assuming the magnetron to be so long that the presence of the end zones may be neglected.

In the next section the effect of the finite length and end zones will be discussed.

Table I

Resonant Modes of Three Vane Magnetrons

1. Model of the Columbia University Radiation Laboratory M-4 magnetron. Scale factor = 7.55

r_1 = 1.728 cm. r_2 = 3.26 cm. r_3 = .957 cm.
Anode length = 4.18 cm. ϕ = .100 N = 14

n	λ(Eq.(I-8'))	λ(Eq.(I-11))	λ(exp.)	% diff.
2	10.62 cm.	11.20 cm.	10.986 cm.	-1.8%
3	9.68	9.84	9.618	-2.2%
4	9.31	9.32	9.096, 9.140	---
5	9.17	9.17	8.904	-3.0%
6	8.96	8.96	8.768	-2.3%
7	8.90	8.90	8.684	-2.5%

2. Model of the Westinghouse VA-1 magnetron. Scale factor = 3.43

r_1 = 1.73 cm. r_2 = 3.45 cm. r_3 = .550 cm.
Anode length = 3.36 cm. ϕ = .0986 N = 18

n	λ(Eq. I-8')	λ(exp.)	% diff.
2	11.92 cm.	12.122 cm.	+1.7%
3	10.80	10.670	-1.3%
4	10.38	10.146, 10.115	-2.4%
5	10.05	9.857, 9.793	---
6	9.96	9.660, 9.633	-3.3%
7	9.84	9.557	-3.0%
8	9.78	9.480	-3.1%
9	9.75	9.457	-3.1%

Table I (continued)

3. Magnetron described by Okress and Wang, P. 11, Radar Memo B-1, Westinghouse Research Laboratories.

r_1 = .68 cm. r_2 = 1.950 cm. r_3 = .24 cm.

Anode length = .64 cm. ϕ = .159 N = 8

n	λ(Eq. I-8')	
1	10.21	
2	8.88	Operating Wave Length
3	8.50	8.05 cm.
4	8.40	

II. The Effect of End Zones

This section presents the results of several attempts to take into account the finite length of the oscillators and the cavities at the ends.

To simplify the problem the circular magnetron is developed into a linear one, details of which are shown in Fig. 3. The linear magnetron may be continued indefinitely in the y-direction, in which case it will act as a waveguide with a band of propagated wave lengths. On the other hand, it may be converted into a cavity by means of end plates in the xz plane. Such a linear magnetron will resonate only at a discrete set of frequencies determined by the requirement that the distance between the end plates be an integral number of half wave lengths in the y-direction. The modes will be labeled in accordance with the notation used for rectangular resonators. They will be designated by three indices ℓ, m, n giving the number of anti-nodes of the field in the x, y, and z directions respectively when the end cavities are reduced to zero. In all the following cases $\ell = 0$. Magnetrons operate in one of the (0,m,1) modes. The (0,m,2) modes are characterized by a node in the z = 0 plane, and are generally of much higher frequency. They have been detected by Slater[2] and Tonks and Crawford[3]. The (0,m,3); (0, m, 4) etc., modes have still higher frequencies.

The cavity may be considered as a special case of the linear magnetron used as a wave guide, for the effect of the end plates can be

---

[2] J. C. Slater, Radiation Laboratory Report 43-9.

[3] L. Tonks and S. N. Crawford, General Electric Research Laboratories, report dated 7/15/42.

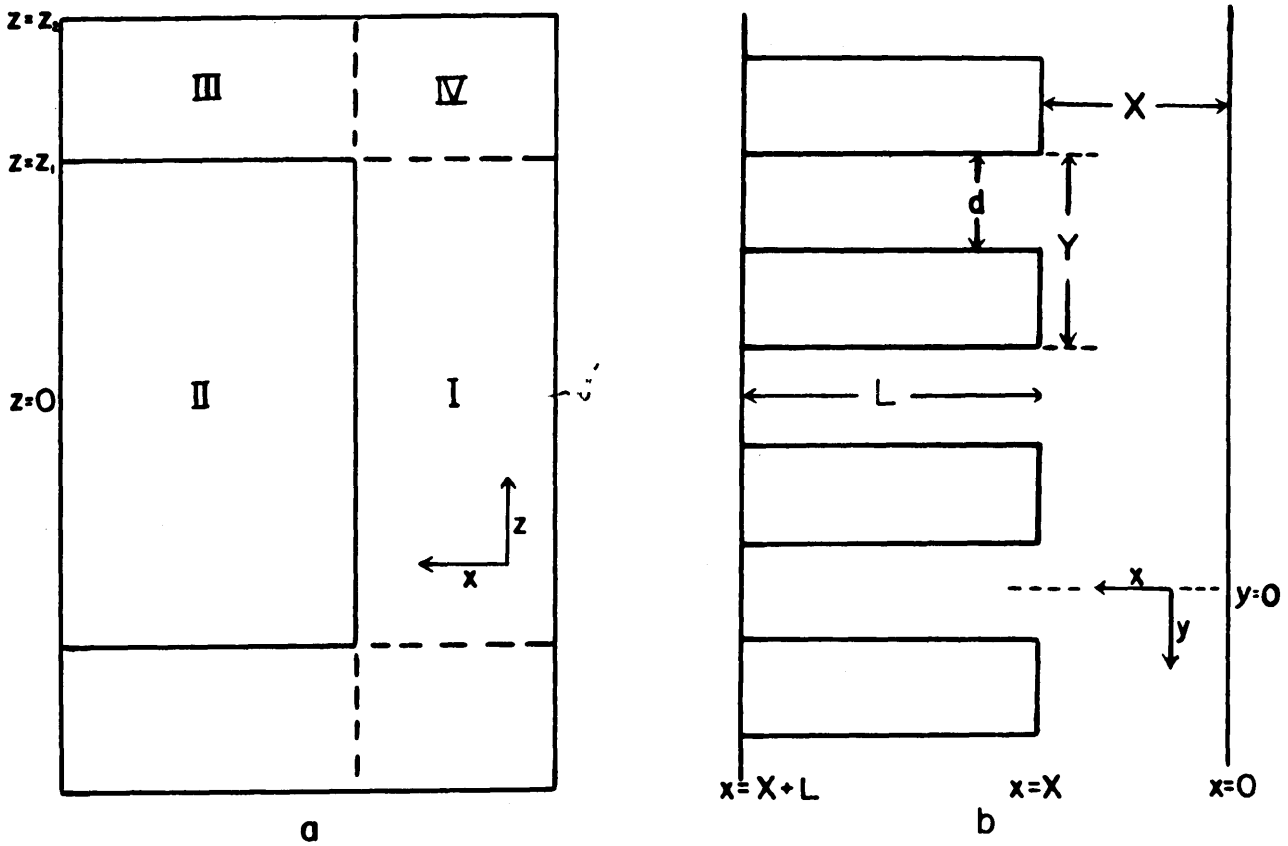

a

Section

b

Plan

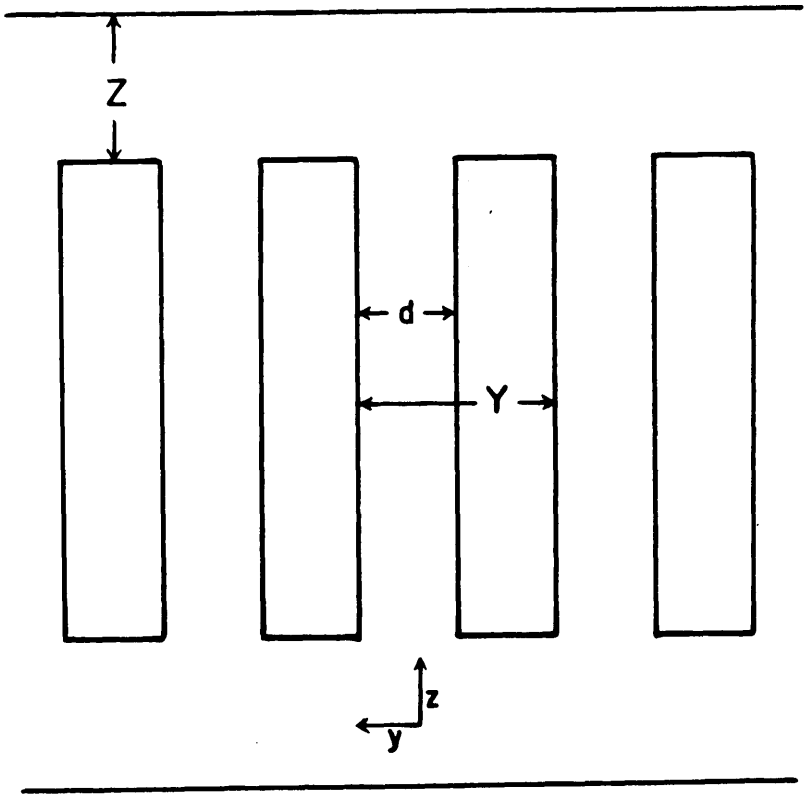

c

Elevation

Fig. 3

reproduced by an infinite set of images. The only distinction between the two is that the wave length in the y-direction in the cavity is limited to certain values.

The space will be divided into four regions as shown in Fig. 3a. Regions III and IV constitute the end cavity or zone, Region II the oscillator cavity, and Region I corresponds to the cavity between the cathode and anode. The fields in IV must be small and will not be considered explicitly. The method will be to set up appropriate solutions for the fields in Regions I, II, and III and then connect or join them one to another.

The appropriate solutions in Region I are traveling waves propagated in the +y and -y directions. Since the wave number in the y-direction, k_{ym}, is always larger than the wave number, k, in empty space, the wave number in the x-direction must be imaginary. The relevant components of the fields in I are

$$\left.\begin{aligned} B_z &= \sum_{-\infty}^{+\infty} a_m e^{iK_{ym}y} \cosh K_{xm}x \cos K_z z \\ E_y &= -\sum_{-\infty}^{+\infty} a_m \frac{i\omega K_{xm}}{K_x'^2} e^{iK_{ym}y} \sinh K_{xm}x \cos K_z z \\ B_y &= -\sum_{-\infty}^{+\infty} a_m \frac{iK_z K_{ym}}{K_x'^2} e^{iK_{ym}y} \cosh K_{xm}x \sin K_z z \end{aligned}\right\} \quad (II-1)$$

with the condition

$$K_{ym}^2 + K_z^2 - K_{xm}^2 = K^2 \qquad (II-2)$$

and where $k^2-k_z^2$ has been designated by $k_x'^2$. The fields are transverse electric in the z-direction, i. e., $E_z = 0$. It has been shown by Slater[4]

---

[4] J. C. Slater, Radiation Laboratory Report V5S P.22-30

that the periodicity of the fields in the oscillator cavities requires the following relation between k_{ym} and k_{yo}:

$$k_{ym} = k_{yo} + \frac{2\pi m}{Y} \qquad m = 0, \pm 1, \pm 2, \pm 3 \ldots\ldots \qquad (II - 3)$$

where Y is the distance between oscillators. From this Slater has also shown that as the maximum value of k_{yo} is π/Y, and the corresponding maximum wave length in the y-direction is 2Y. If the linear magnetron is used as a waveguide k_{yo} may take any value between 0 and π/Y. If used as a cavity the possible values of k_{yo} are $\frac{m\pi}{NY}$, m = 1,2, . . . N; where N is the number of oscillators contained in the length of the cavity. The fields of Eq. (II-1) are suitable for that type of mode in which the index n is odd. If the index n is even cos $k_z z$ is replaced by sin $k_z z$, and sin $k_z z$ by -cos $k_z z$.

Some of the components in the jth slot are:

$$B_{zj} = b_o e^{ik_{yo}jY} \cos k_x'(x - X - L) \cos k_z z + \sum_1^\infty b_m e^{ik_{yo}jY} \cos \frac{m\pi}{d}(y' + \tfrac{d}{2}) \cosh k_{xm}'(x - X - L) \cos k_z z + \sum_1^\infty d_m e^{ik_{yo}jY} \cos \frac{m\pi}{d}(y' + \tfrac{d}{2}) \cos k_x'(x - X - L) \cosh k_{zn}' z \qquad (II - 4)$$

$$E_{yj} = \frac{i\omega}{k_x'} b_o e^{ik_{yo}jY} \sin k_x'(x - X - L) \cos k_z z - \sum_1^\infty \frac{i\omega}{k_x'^2} k_{xm}' b_m e^{ik_{yo}jY} \cos \frac{m\pi}{d}(y' + \tfrac{d}{2}) \sinh k_{xm}'(x - X - L) \cos k_z z + \sum_1^\infty \frac{i\omega}{k_x'} d_m e^{ik_{yo}jY} \cos \frac{m\pi}{d}(y' + \tfrac{d}{2}) \sin k_x'(x - X - L) \cosh k_{zm}' z$$

where

$$\gamma' = \gamma - j\Upsilon$$

and

$$\left(\frac{m\pi}{d}\right)^2 - k'^2_{xm} = k'^2_x$$

$$\left(\frac{m\pi}{d}\right) - k'^2_{zm} + k'^2_x = k^2 \qquad (II-5)$$

The first term in each field corresponds to the principal mode; the second term contains the higher modes generated at the edges of the slot at x = X, which decay exponentially in the interior of the oscillator cavity. The third term likewise contains higher modes, due here to the edges at the top of the slot at $z = z_1$.

The fields in I and II are connected by making some reasonable assumption as to the form of E_y across the slot at x = X. The coefficients a_m, b_m, and d_m, which are essentially coefficients of a Fourier expansion, are then determined. The higher modes generated at the top edges are almost zero except for z close to $+ z_1$, and may therefore be neglected in performing this joining. Since the fields in I and II then depend in the same way on z, this z dependence will drop out. The joining is completed by requiring that the tangential magnetic field, averaged in some fashion, be continuous across the slot in the x = X plane. This requirement results in an equation connecting the wave numbers in the two regions. Examination of the fields shows that this relation may be written explicitly in terms of k_{yo} and k_x' alone. That is, it will have the form

$$f(k'_x, k_{yo}) = 0 \qquad (II-6)$$

Hence given k_{yo} (and for a cavity that is equivalent to specifying the m

index) then k_x' is determined independently of the variation in the z-direction. The resonant frequency can then be found from

$$k^2 = k_x'^2 + k_z^2$$

If the magnetron is of indefinite extent in the z-direction then $k_z=0$ and $k=k_x'$. Another limiting case occurs when Z=0, i. e., no end zones. The frequency is then given by

$$k^2 = k_x'^2 + \left(\frac{n\pi}{2z_1}\right)^2 \qquad (II-7)$$

where n is the third index of the mode, and $2z_1$ the height of the oscillator cavities.

The particular expression to be used in Eq. (II-6) depends on the assumed form of the electric field across the slot. If the edge effects are completely neglected, and hence E_y is constant across the slot, then Slater[5] has found that the relation is:

$$\frac{d}{Y}\sum_{-\infty}^{+\infty}\frac{k_x'}{k_{xm}}\frac{\tan k_x' L}{\tanh k_{xm} X}\left(\frac{\sin k_{ym}d/2}{k_{ym}d/2}\right)^2 - 1 = 0 \qquad (II-8)$$

The edge effects may be included to a high degree of approximation if one assumes the field which is calculated from the solution of the electrostatic problem. In treating the problem of a T-joint in a wave guide Frank and Chu[6] have suggested a field closely approximating the electrostatic solution which is of the following form:

$$E_y(X) = \frac{Ae^{ik_{yo}jY}\cos k_z z}{\sqrt{1-\left(\frac{2y'}{d}\right)^2}} + \frac{2y'}{d}\frac{Ce^{ik_{yo}jY}\cos k_z z}{\sqrt{1-\left(\frac{2y'}{d}\right)^2}} \qquad (II-9)$$

The coefficients a_m, b_m of Eqs. (II-1) and (II-4) are determined in terms of A and C. The average of the tangential magnetic field may then be calculated in each region, and must join on at x=X. Similarly the averages

---

[5] J. C. Slater, Radiation Laboratory Report V5S P. 28

[6] N. H. Frank and L. J. Chu, Radiation Laboratory Report 43-6

with respect to the first Fourier component, $\sin \frac{\pi y'}{d}$, must be equal at $x = X$. These two conditions result in two linear homogeneous equations for A and C. Eq. (II-6) is then given by the requirement that these equations have a non-vanishing solution.

The coefficients a_m must be such that E_y satisfies the boundary conditions on the walls and at the slots. These are

$$-\sum \frac{i\omega k_{xm}}{k_x'^2} a_m e^{ik_{ym}y} \sinh k_{xm} X = 0, \qquad (j-1)Y + d/2 < y < jY - d/2$$

$$= \frac{A e^{ik_{yo} jY}}{\sqrt{1-(\frac{2y'}{d})^2}} + \frac{2y'}{d} \frac{C e^{ik_{yo} jY}}{\sqrt{1-(\frac{2y'}{d})^2}}, \qquad (II-10)$$

$$jY - d/2 < y < jY + d/2$$

If both sides are multiplied by $e^{-ik_{yn}Y}$ and integrated between $(j - \frac{1}{2})Y$ and $(j + \frac{1}{2})Y$, the equation becomes:

$$-\sum_{-\infty}^{+\infty} \frac{i\omega k_{xm}}{k_x'^2} a_m \sinh k_{xm} X \int_{(j-\frac{1}{2})Y}^{(j+\frac{1}{2})Y} e^{2\pi i \frac{m-n}{Y} y} dy$$

$$= \int_{-\frac{d}{2}}^{+\frac{d}{2}} \frac{A + \frac{2y'}{d} C}{\sqrt{1-(\frac{2y'}{d})^2}} e^{ik_{yn}y'} dy'$$

or

$$-\frac{i\omega k_{xn}}{k_x'^2} a_n Y \sinh k_{xn} X = A \int_{-\frac{d}{2}}^{+\frac{d}{2}} \frac{\cos k_{yn} y' dy'}{\sqrt{1-(\frac{2y'}{d})^2}} - iC \int_{-\frac{d}{2}}^{+\frac{d}{2}} \frac{\frac{2y'}{d} \sin k_{yn} y' dy'}{\sqrt{1-(\frac{2y'}{d})^2}}. \qquad (II-11)$$

These integrals may be evaluated by changing the variable to $\theta = \arcsin \frac{2y'}{d}$

and using the expansion of $e^{i\rho \sin\theta}$ in Bessel functions[7]. The final expression is

$$a_n = -\frac{k_x'^2}{i\omega k_{xn}} \frac{\pi}{2} \frac{d}{Y} \frac{A J_0(k_{yn} d/2) - i C J_1(k_{yn} d/2)}{\sinh k_{xn} X} \qquad (II-12)$$

The expansion coefficients, b_m, in II are found similarly:

$$-\frac{i\omega}{k_x'} b_0 d \sin k_x' L = \int_{-d/2}^{+d/2} \frac{A + \frac{2y'}{d} C}{\sqrt{1-\left(\frac{2y'}{d}\right)^2}} dy'$$

or

$$b_0 = -\frac{\pi}{2} \frac{k_x' A}{i\omega \sin k_x' L} \qquad (II-13)$$

and

$$b_m = \frac{k_x'^2}{i\omega} \frac{2}{d k_{xm}' \sinh k_{xm}' L} \int_{-d/2}^{+d/2} \frac{\left(A + \frac{2y'}{d} C\right) \cos \frac{m\pi}{d}\left(y' + \frac{d}{2}\right)}{\sqrt{1-\left(\frac{2y'}{d}\right)^2}} dy'$$

Here two cases must be distinguished. If m is odd,

$$b_m = -\pi \frac{k_x'^2}{i\omega} \frac{C J_1(m\pi/2)}{k_{xm}' \sinh k_{xm}' L} \qquad m \text{ odd}$$

and if m is even,

$$b_m = \pi \frac{k_x'^2}{i\omega} \frac{A J_0(m\pi/2) \cos m\pi/2}{k_{xm}' \sinh k_{xm}' L} \qquad m \text{ even} \qquad (II-14)$$

With these coefficients the z-component of the magnetic field in Region I is:

$$B_z(x) = -\frac{d}{Y} \frac{\pi}{2} \sum_{m=-\infty}^{+\infty} \frac{k_x'^2}{i\omega k_{xm}} e^{i k_{ym} y} \left(A J_0(k_{ym} d/2) - i C J_1(k_{ym} d/2)\right) \frac{\cos k_z z \cosh k_{xm} x}{\sinh k_{xm} X}$$

The average of this component across the jth slot is then

$$\overline{B_z}(X) = -\frac{d}{Y} \frac{\pi}{2} \sum_{-\infty}^{+\infty} \frac{k_x'^2}{i\omega k_{xm}} e^{i k_{yo} j y} \frac{A J_0(k_{ym} d/2) - i C J_1(k_{ym} d/2)}{\tanh k_{xm} X} \cos k_z z \frac{\sin k_{ym} d/2}{k_{ym} d/2}, \qquad (II-15)$$

---

[7] J. A. Stratton, "Electromagnetic Theory," McGraw Hill, New York, P. 372

and the similar average, weighted by the Fourier component, $\sin \frac{\pi y'}{d}$, is given by

$$\overline{\overline{B}}_z(X) = \frac{1}{d}\int_{-d/2}^{+d/2} B_z \sin\frac{\pi y'}{d}\, dy'$$

or

$$\overline{\overline{B}}_z(X) = -i\frac{d}{Y}\sum_{-\infty}^{+\infty}\frac{\pi}{2}\frac{k_x'^2}{i\omega k_{xm}} e^{ik_{yo}jY}\frac{AJ_o(k_{ym}d/2) - iCJ_1(k_{ym}d/2)}{\tanh k_{xm}X}\frac{k_{ym}d/2\cos k_{ym}d/2}{(\pi/2)^2 - (k_{ym}d/2)^2}. \quad (II-16)$$

These are to be set equal to the corresponding averages of the field in II, which are in fact just the first two terms of the field, and there results:

$$\frac{d}{Y}\sum_{-\infty}^{+\infty}\frac{k_x'}{k_{xm}}\frac{AJ_o(k_{ym}d/2) - iCJ_1(k_{ym}d/2)}{\tanh k_{xm}X}\frac{\sin k_{ym}d/2}{k_{ym}d/2} = \frac{A}{\tan k_x' L}$$

$$-i\frac{d}{Y}\sum_{-\infty}^{+\infty}\frac{1}{k_{xm}}\frac{AJ_o(k_{ym}d/2) - iCJ_1(k_{ym}d/2)}{\tanh k_{xm}X}\frac{k_{ym}d/2\cos k_{ym}d/2}{(\pi/2)^2-(k_{ym}d/2)^2} = \frac{CJ_1(\pi/2)}{k_{x_1}'\tan k_{x_1}' L} \quad (II-17)$$

Imposing the condition that these two equations have non-vanishing solutions yields the desired relation between k_{yo} and k_x':

$$\begin{vmatrix}\alpha & \beta\\ \gamma & \delta\end{vmatrix} = 0 \quad (II-18)$$

where

$$\alpha = \frac{d}{Y}\sum\frac{k_x'}{k_{xm}}\frac{\tan k_x' L}{\tanh k_{xm}X}J_o(k_{ym}d/2)\frac{\sin k_{ym}d/2}{k_{ym}d/2} - 1$$

$$\beta = \frac{d}{Y}\sum\frac{k_x'}{k_{xm}}\frac{\tan k_x' L}{\tanh k_{xm}X}J_1(k_{ym}d/2)\frac{k_{ym}d/2\cos k_{ym}d/2}{(\pi/2)^2-(k_{ym}d/2)^2}$$

$$\gamma = \frac{d}{Y}\sum\frac{k_{x_1}'\tanh k_{x_1}' L}{k_{xm}\tanh k_{xm}X}J_o(k_{ym}d/2)\frac{\sin k_{ym}d/2}{k_{ym}d/2}$$

and

$$\delta = \frac{d}{Y} \sum \frac{k'_{x1} \tanh k'_{x1} L}{k_{xm} \tanh k_{xm} X} J_1\left(k_{ym} d/2\right) \frac{k_{ym} d/2 \cos k_{ym} d/2}{(\pi/2)^2 - (k_{ym} d/2)^2} + J_1(\pi/2)$$

For k_{yo} large the cross terms β and γ' are small, vanishing identically when $k_{yo} = \frac{\pi}{Y}$. Hence the roots of Eq. (II-18) are practically the roots of $\alpha = 0$, which differs from Eq. (II-8), derived by Slater, only in having $\left(\frac{\sin k_{ym} d/2}{k_{ym} d/2}\right)^2$ replaced by $J_o(k_{ym} d/2) \frac{\sin k_{ym} d/2}{k_{ym} d/2}$. This difference does not appreciably affect the first few terms of the series.

Table II compares the values of k', for several different values of k_{yo}, as obtained first from Eq. (II-8) and secondly from Eq. (II-18).

Table II

$k_{yo} = \frac{m\pi}{10Y}$, L = 1.753 cm., X = 1.905 cm., Y = .953 cm., $\frac{d}{Y} = .5$

m	k_x'(Eq. II-8)	k_x'(Eq. II-8)	% diff.	C/A
1	.2673 $cm.^{-1}$	.2690 $cm.^{-1}$	+.64	1.21
5	.7320	.7392	+.98	.21
8	.7736	.7810	+.96	.062
10	.7792	.7868	+.98	.000

The difference is at all times less than 1%. For small k_{yo} the difference arises chiefly from the cross terms β and γ', while for large k_{yo} it is due to the change in α. This is also shown by the last column in Table II which gives the relative strength of the antisymmetric portion of the field.

There is some experimental evidence, to be presented later that the method used here "over corrects" for edge effects and that the true value lies somewhere between the solutions of Eq. (II-8) and of (II-18). This is to be expected since the assumed field has an infinity of the 1/2 order at the slot edge, which is stronger than the infinity of 1/3 order of the more correct electrostatic field.

The problem of the effect of the end zones has now been reduced to finding k_z, which is to be determined by the fields in III and the manner in which they are joined on to the fields in other regions. Several ways have been tried.

Method A The simplest method is to proceed in the same manner as was done for Regions I and II. Set up solutions in III similar to those in I; i.e., waves traveling in the y-direction, and decaying almost exponentially in the z-direction. Choosing the same tangential electric field at the top slot, the Fourier coefficients are fixed, and k_z is found by matching the tangential magnetic field.

The fields in III are chosen transverse electric to the x-direction. The components which are needed are:

$$\left.\begin{aligned} B_x &= \sum_{-\infty}^{+\infty} c_m e^{i k_{ym} y} \sin k_x'(x - X - L) \cosh k_{zm}''(z - z_2) \\ E_y &= \sum_{-\infty}^{+\infty} \frac{i\omega k_{zm}''}{k_z^2} c_m e^{i k_{ym} y} \sin k_x'(x - X - L) \sinh k_{zm}''(z - z_2) \end{aligned}\right\} \quad (II-19)$$

where

$$k_{ym}^2 - k_{zm}''^2 = k^2 - k_x'^2 = k_z^2$$

It is evident that the wave numbers in the y-direction must be the same as those in Region I in order that the fields have the same periodicity

as the fields in the oscillator cavities. The fields in Region II are the same as in Eq. (II-4), except that now the higher modes set up near the edges at x = X may be neglected since they do not penetrate appreciably into the oscillator cavity.

$$\left.\begin{aligned} B_x &= b_0 e^{i k_{yoj} Y} \sin k_x'(x-X-L) \sin k_z z \\ &\quad + \sum_1^\infty d_m \cos \frac{m\pi}{d}(y'+d/2)\, e^{i k_{yoj} Y} \sin k_x'(x-X-L) \sinh k_{zm}' z, \\ E_y &= \frac{i\omega}{k_z} b_0 e^{i k_{yoj} Y} \sin k_x'(x-X-L) \cos k_z z \\ &\quad + \sum \frac{i\omega k_{zm}'}{k_z^2} d_m \cos m\frac{\pi}{d}(y'+d/2)\, e^{i k_{yoj} Y} \sin k_x'(x-X-L) \cosh k_{zm}' z. \end{aligned}\right\} \quad (II\text{-}20)$$

We assume that the field across the slot at $z = + z_1$ is

$$E_y(z_1) = \frac{A + 2y'/d\, C}{\sqrt{1-(2y'/d)^2}}\, e^{i k_{yoj} Y} \sin k_x'(x-X-L)$$

The Fourier coefficients are then:

$$C_m = -\frac{\pi}{2}\frac{d}{Y}\frac{k_z^2}{i\omega k_{zm}''} \frac{A J_0(k_{ym} d/2) - i C J_1(k_{ym} d/2)}{\sinh k_{zm}'' Z},$$

where $Z = z_1 - z_2$, the height of the end zone,

$$\left.\begin{aligned} b_0 &= \frac{\pi}{2}\frac{k_z}{i\omega}\frac{A}{\cos k_z z_1}, \\ b_1 &= -\pi \frac{k_z^2}{i\omega} \frac{C J_1(\pi/2)}{k_{z1}' \cosh k_{z1}' z_1}, \end{aligned}\right\} \quad (II\text{-}21)$$

and so on. We now find the average of the tangential magnetic field, B_x, in III and set it equal, at the slot, to the corresponding average in II:

$$-\frac{d}{Y}\sum \frac{k_z^2}{k_{zm}''} \frac{A J_0(k_{ym} d/2) - i C J_1(k_{ym} d/2)}{\tanh k_{zm}'' Z} \frac{\sin k_{ym} d/2}{k_{ym} d/2} = A k_z \tan k_z z_1,$$

Similarly, joining the averages with respect to $\sin \frac{xy'}{d}$ we have:

$$-i \frac{d}{Y} \sum_{-\infty}^{+\infty} \frac{K'_{z1}}{K_z} \frac{A J_0(K_{ym} d/2) - i C J_1(K_{ym} d/2)}{\tanh K''_{zm} Z} \frac{K_{ym} d/2 \cos K_{ym} d/2}{(\frac{\pi}{2})^2 - (K_{ym} d/2)^2} = C J_1(\tfrac{\pi}{2}) \tanh K'_{z1} z_1.$$

The condition that these equations have a non-vanishing solution is:

$$K_z^2 \begin{vmatrix} \alpha & \beta \\ \gamma & \delta \end{vmatrix} = 0 \qquad (II-22)$$

where now

$$\alpha = \frac{d}{Y} \sum_{-\infty}^{+\infty} \frac{K_z \cot K_z z_1}{K''_{zm} \tanh K''_{zm} Z} J_0(K_{ym} d/2) \frac{\sin K_{ym} d/2}{K_{ym} d/2} + 1$$

$$\beta = \frac{d}{Y} \sum \frac{K_z \cot K_z z_1}{K''_{zm} \tanh K''_{zm} Z} J_1(K_{ym} d/2) \frac{\sin K_{ym} d/2}{K_{ym} d/2}$$

$$\gamma = \frac{d}{Y} \sum \frac{K'_{z1} \coth K'_{z1} z_1}{K''_{zm} \tanh K''_{zm} Z} J_0(K_{ym} d/2) \frac{K_{ym} d/2 \cos K_{ym} d/2}{(\frac{\pi}{2})^2 - (K_{ym} d/2)^2}$$

$$\delta = \frac{d}{Y} \sum \frac{K'_{z1} \coth K'_{z1} z_1}{K''_{zm} \tanh K''_{zm} Z} J_1(K_{ym} d/2) \frac{K_{ym} d/2 \cos K_{ym} d/2}{(\frac{\pi}{2})^2 - (K_{ym} d/2)^2} + J_1(\tfrac{\pi}{2})$$

This is valid if the third index of the mode, n, is an odd integer. If n is even, $\cot k_z z_1$ is replaced by $-\tan k_z z_1$ and $\coth k'_{z1} z_1$ by $\tanh k'_{z1} z_1$.

Again the cross-terms β and γ are very small, so that the vanishing of the determinant depends on either α or δ changing sign. But δ is always positive, and α does not change sign providing $k_z z_1 < \frac{\pi}{2}$. This means that for the (0,m,1) type of mode the only solution is $k_z = 0$, which corresponds to zero end effect, no matter how small the end zone. Such a prediction is obviously at variance with the facts. For the (0,m,2) and (0,m,3) modes solutions of Eq. (II-22), other than $k_z = 0$, exist. The calculated resonant wave length, $\lambda = 2\pi/\sqrt{k_x'^2 + k_z^2}$, for a 10 slot linear magnetron is plotted in Figs. 4 and 5 as function of the size of

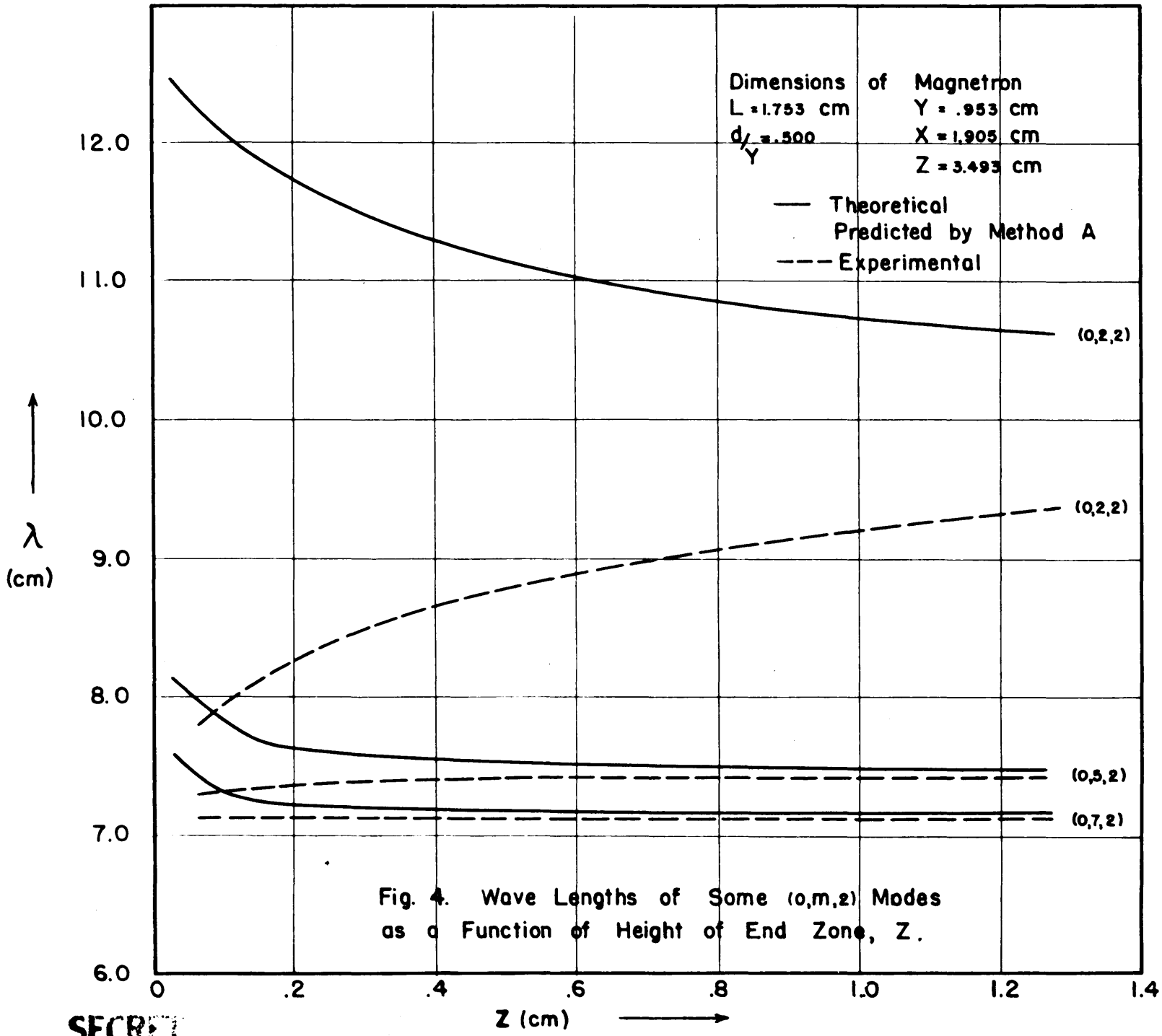

Fig. 4. Wave Lengths of Some (0,m,2) Modes as a Function of Height of End Zone, Z.

M. I. T. RADIATION LAB. DWG. NO. X - 2408-A

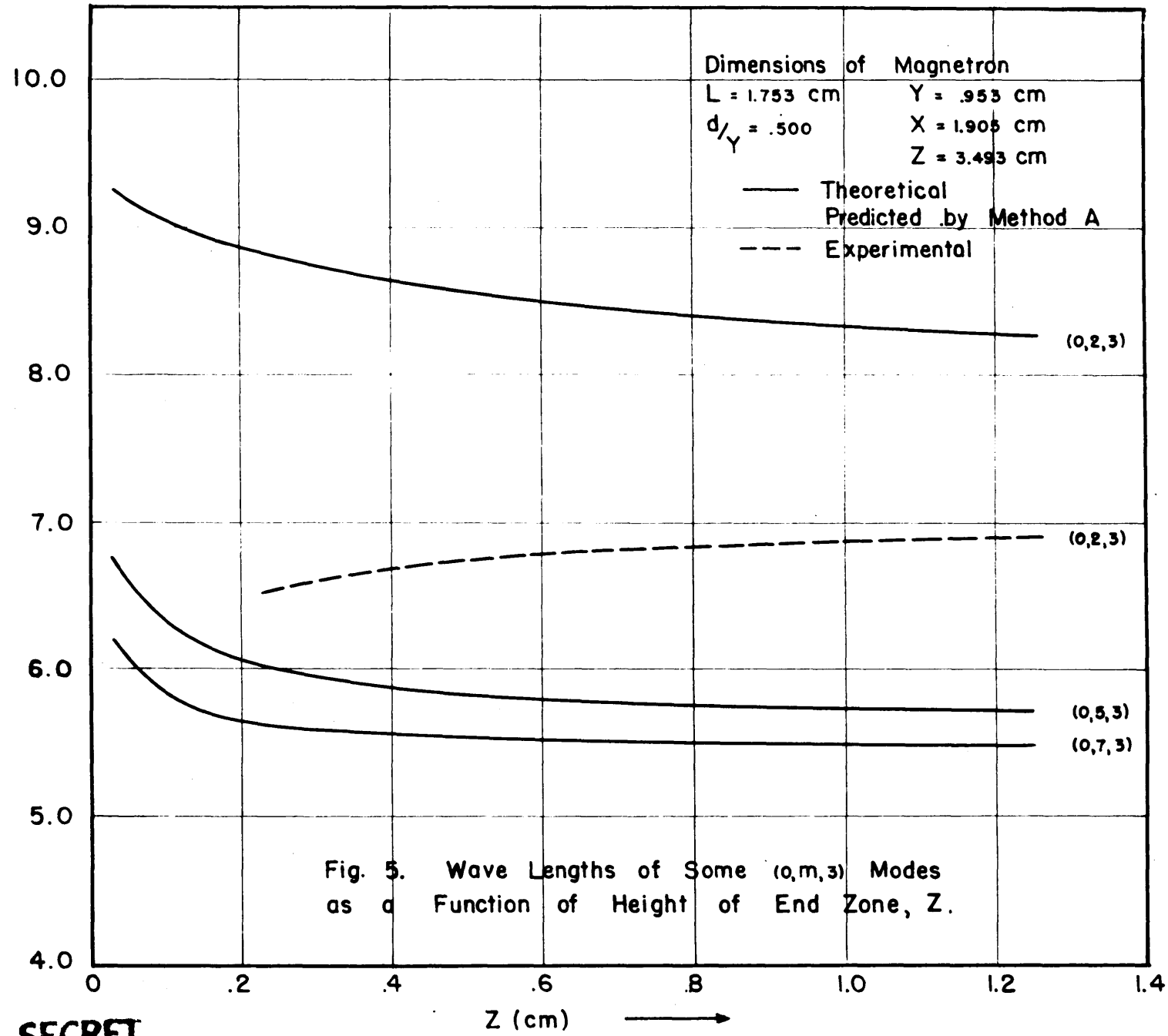

Fig. 5. Wave Lengths of Some (0,m,3) Modes as a Function of Height of End Zone, Z.

M. I. T. RADIATION LAB. DWG. NO. X-[illegible]

SECRET

the end zone, Z, for several values of m. Also shown are the results of experiments on such a linear magnetron, to be discussed in the next section. The predicted values do not agree qualitatively with experiment, since the measured wave length decreases as $Z \to 0$ whereas Eq. (II-22) predicts increasing wave length. For large Z there is surprisingly good quantitative agreement for the (0,5,2) and the (0,7,2) modes. This agreement must be considered accidental, for it is at such values of k_z that $\tan k_z z_1$ is almost infinite. In general the method outlined does not yield a satisfactory solution of the problem.

Method B The second method tried is essentially a variant of method A and will not be discussed in detail. It considers the problem as one of a wave guide with a periodic array of T-joints. The fields in the oscillator cavities are the same as those previously used except that the antisymmetrical component is neglected. In the end zone 'partial' fields, corresponding to each slot, are set up such that the tangential electric field of each partial field matches the field in the slot and vanishes everywhere else in the $z = z_1$ plane. At large distances from its slot each partial tangential magnetic field has the form of a traveling wave corresponding to a $(T.E.)_{1,0}$ mode propagated in the end zone. In addition there are higher modes generated at the edges of the slot which decay rapidly away from the slot. The total magnetic field is the sum of these partial fields and the average of this total field

is matched to the field in Region II. The final equation determining k_z is:

$$0 = k_z^2 \left\{ \frac{\tan k_z z_1}{k_z} - \frac{1}{k_z \tan k_z Z} + \frac{J_0(k_z d/2)\cos k_z d/2}{k_z^2 Z} \right.$$

$$+ \frac{\sin k_z d/2\, J_0(k_z d/2)}{k_z^2 Z} \frac{\sin k_z Y}{1+\cos k_z Y} + 2\sum_1^\infty \frac{e^{-\frac{n\pi d}{2Z}} I_0\left(\frac{n\pi d}{2Z}\right)}{\frac{n^2\pi^2}{Z}} \qquad \text{(II-23)}$$

$$\left. + 4\sum_1^\infty \frac{e^{-\frac{n\pi Y}{Z}} I_0\left(\frac{n\pi d}{2Z}\right) \sinh \frac{n\pi d}{2Z}}{n^2\pi^2/Z\,(1+2e^{-n\pi Y/Z})} \right\},$$

where I_0 is the zeroth order modified Bessel function. This equation has no root less than $\pi/2z_1$ except $k_z = 0$, as with the previous method. Table III compares the results of this equation for the (0,10,2) mode with the results of Method A. Considering the difference in the manner of setting

Table III

(0, 10, 2) mode. Dimensions as in Table II

Z	k_z(Eq. II-22)	k_z(Eq. II-23)
.02 cm.	.244 cm.$^{-1}$	.245
.04	.307	.306
.08	.359	.359
.20	.403	.403
1.00	.421	.417

up the fields, the close agreement is surprising. This method thus yields nothing new.

Method C In the previous methods the fields in the end zone are connected with those in I only indirectly, through the oscillator cavities. Yet the end zones and Region I really form a continuous region. Region III can be considered as a part of I that has been bent at 90°. The error of the previous methods must lie in the omission of a factor insuring the continuity of these regions.

The simplest way of directly connecting Regions I and II is to require the continuity of the tangential magnetic field, B_y, at the junction of the two regions, namely, at the edge of the vanes defined by $z = z_1$ and $x = X$. This condition has some simple physical interpretations. It states that the electric potential of the edge is the same whether approached from Region III or Region I. Equivalently, it requires that the currents along the face of the vanes in the z-direction join on smoothly to the currents in the x-direction along the top of the vanes. It is easy to see that this condition results in a qualitatively correct answer. If the tangential electric field E_y is properly matched between II and III, it can be shown simply from Maxwell's equations that the vertical component of B is also matched. It then follows from div B = 0 that the flux of B_z at the boundary between II and III is equal to the flux of B_y in III, minus the small amount of flux of B_x 'leaking' from III into IV. Since the ratio of B_x to B_y is very small when k_z is small, approximately $\frac{k_z^2}{k_{yo}k_x}$, this leakage flux is negligible. Hence the flux of B_z in the oscillator cavities is 'converted' almost entirely into flux of B_y in III. As Z decreases, the same amount of flux is crowded into a smaller area, and therefore B_y must increase. Since B_y in I

varies as sin $k_z z$, that requires k_z to increase as Z becomes smaller. This is in rough agreement with experiment.

The calculation of k_z according to this procedure will be carried out omitting edge effects, i. e., the fields in the oscillator cavities will be assumed constant across the width of the slot. The field components that are needed are;

in Region I:

$$\left.\begin{aligned} B_z &= \sum_{-\infty}^{+\infty} a_m e^{i k_{ym} y} \cosh k_{xm} x \cos k_z z \\ B_y &= \sum_{-\infty}^{+\infty} \frac{i k_z k_{ym}}{k_x'^2} a_m e^{i k_{ym} y} \cosh k_{xm} x \sin k_z z \\ E_y &= \sum_{-\infty}^{+\infty} \frac{i \omega k_{xm}}{k_x'^2} a_m e^{i k_{ym} y} \sinh k_{xm} x \cos k_z z \end{aligned}\right\} \quad (II-24)$$

in the jth oscillator cavity:

$$\left.\begin{aligned} B_{xj} &= b_o e^{i k_{yo} j Y} \sin k_x' (x - X - L) \sin k_z z \\ B_{zj} &= \frac{k_x'}{k_z} b_o e^{i k_{yo} j Y} \cos k_x' (x - X - L) \cos k_z z \\ E_{yj} &= \frac{i\omega}{k_z} b_o e^{i k_{yo} j Y} \sin k_x' (x - X - L) \cos k_z z \end{aligned}\right\} \quad (II-25)$$

and in Region III:

$$\left.\begin{aligned} B_x &= \sum_{-\infty}^{+\infty} c_m e^{i k_{ym} y} \cosh k_{zm}'' (z - z_2) \sin k_x' (x - X - L) \\ B_y &= \sum \frac{i k_{ym} k_x'}{k_z^2} c_m e^{i k_{ym} y} \cosh k_{zm}'' (z - z_2) \cos k_x' (x - X - L) \\ E_y &= \sum \frac{i \omega k_{zm}''}{k_z^2} c_m e^{i k_{ym} y} \sinh k_{zm}'' (z - z_2) \sin k_x' (x - X - L) \end{aligned}\right\} \quad (II-26)$$

The expansion coefficients a_m and c_m are determined as before by matching the tangential component of the electric field, E_y, to the field in the oscillator cavities. The details of this calculation are similar to those in the previous matching between I and II and only the results need

be given:

$$a_m = \frac{d}{Y} b_o \frac{k_x'^2}{k_{xm} k_z} \frac{\sin k_x' L}{\sinh k_{xm} X} \frac{\sin k_{ym} d/2}{k_{ym} d/2}$$

$$c_m = -\frac{d}{Y} b_o \frac{k_z}{k_{zm}''} \frac{\cos k_z z_1}{\sinh k_{zm}'' Z} \frac{\sin k_{ym} d/2}{k_{ym} d/2} \qquad (II-27)$$

With these coefficients B_y in Region I at the edge $z = z_1$, $x = X$ becomes:

$$B_y(z_1, X) = -i \sum_{-\infty}^{+\infty} b_o \frac{k_{ym}}{k_{xm}} \frac{d}{Y} \frac{\sin k_x' L}{\tanh k_{xm} X} \frac{\sin k_{ym} d/2}{k_{ym} d/2} e^{i k_{ym} y} \sin k_z z_1 \qquad (II-28)$$

Since the matching cannot be done exactly, we match the average of B_y across the width of a vane. From Eq. (II-28) this average in Region I is

$$\bar{B}_y = \frac{1}{D} \int_{jY+d/2}^{(j+1)Y-d/2} B_y(z_1, X)\, dy$$

$$= -i \sum_{-\infty}^{+\infty} \frac{d}{Y} b_o \frac{k_{ym}}{k_{xm}} e^{i k_{yo}(j+1/2)Y} e^{\pi m i} \frac{\sin k_x' L}{\tanh k_{xm} X} \frac{\sin k_{ym} d/2}{k_{ym} d/2} \frac{\sin k_{ym} D/2}{k_{ym} D/2} \qquad (II-29)$$

where $D = Y - d$, the width of a vane. Similarly, in Region III B_y at the edge is

$$B_y(z_1, X) = -i \sum_{-\infty}^{+\infty} \frac{d}{Y} b_o \frac{k_{ym}}{k_{zm}''} \frac{k_x'}{k_z} \frac{\cos k_z z_1 \cos k_x' L}{\tanh k_{xm} X} \frac{\sin k_{ym} d/2}{k_{ym} d/2} e^{i k_{ym} y}$$

and the corresponding average is

$$\bar{B}_y = -i \sum_{-\infty}^{+\infty} \frac{d}{Y} b_o \frac{k_{ym}}{k_{zm}''} \frac{k_x'}{k_z} e^{i k_{yo}(j+1/2)Y} e^{\pi m i} \frac{\cos k_x' L}{\tanh k_{xm} X} \frac{\sin k_{ym} d/2}{k_{ym} d/2} \frac{\sin k_{ym} D/2}{k_{ym} D/2}$$

The transcendental equation for k_z is found by equating these two averages:

$$\frac{\tan k_x' L}{k_x'} \sum_{-\infty}^{+\infty} (-1)^m \frac{k_{ym}}{k_{xm} \tanh k_{xm} X} \frac{\sin k_{ym} d/2}{k_{ym} d/2} \frac{\sin k_{ym} D/2}{k_{ym} D/2}$$

$$= \frac{1}{k_z \tan k_z z_1} \sum_{-\infty}^{+\infty} (-1)^m \frac{k_{ym}}{k_{zm}'' \tanh k_{zm}'' Z} \frac{\sin k_{ym} d/2}{k_{ym} d/2} \frac{\sin k_{ym} D/2}{k_{ym} D/2} \qquad (II-30)$$

If Z and the mode index m are large, so that $k_{yo} \simeq k''_{zo} \simeq k_{xo}$ and the hyperbolic tangents are practically 1, then the two series are almost identical and Eq. (II-30) reduces to

$$k_z \tan k_z z_1 = \frac{k_x'}{\tan k_x' L} \quad . \qquad (II-31)$$

Another simple expression can be obtained if k_{yo} is small, since then k_{ym} is approximately $-k_{y,-m}$ and k_{xm} is almost equal to $k_{x,-m}$. In each series the mth term therefore cancels the -mth term, leaving only the zeroth term. When k_{yo} is small

$$\frac{\sin k_{yo} d/2}{k_{yo} d/2} \quad \frac{\sin k_{yo} D/2}{k_{yo} D/2} \simeq 1 \quad ,$$

and the relation between k_{yo} and k_x', Eq. (II-8), can then be written as:

$$\frac{d}{Y} \frac{k_x' \tan k_x' L}{k_{xo} \tanh k_{xo} X} = 1 \quad . \qquad (II-8')$$

With these simplifications Eq. (II-30) becomes

$$k_z \tan k_z z_1 = \frac{d}{Y} \frac{k_x'^2}{k_{zo}''} \coth k_{zo}'' Z \quad , \qquad (II-32)$$

where $k_{zo}'' = \sqrt{k_{yo}^2 - k_z^2}$

The calculated wave lengths of some (0,m,1) modes in a 10 slot linear magnetron are plotted in Fig. 6 as a function of end zone height Z. They are computed from Eqs. (II-18) and II-30). Also plotted are the experimentally measured wave lengths. Fig. 7 is a similar plot for (0,m,2) modes. The agreement is qualitatively correct since the calculated wave lengths decrease with decreasing Z, but the calculated values are always too small. When the mode index m is small, the wave lengths disagree by about 4%. Since the measured end effect is only 8% at large Z for these modes, the relative error is quite large.

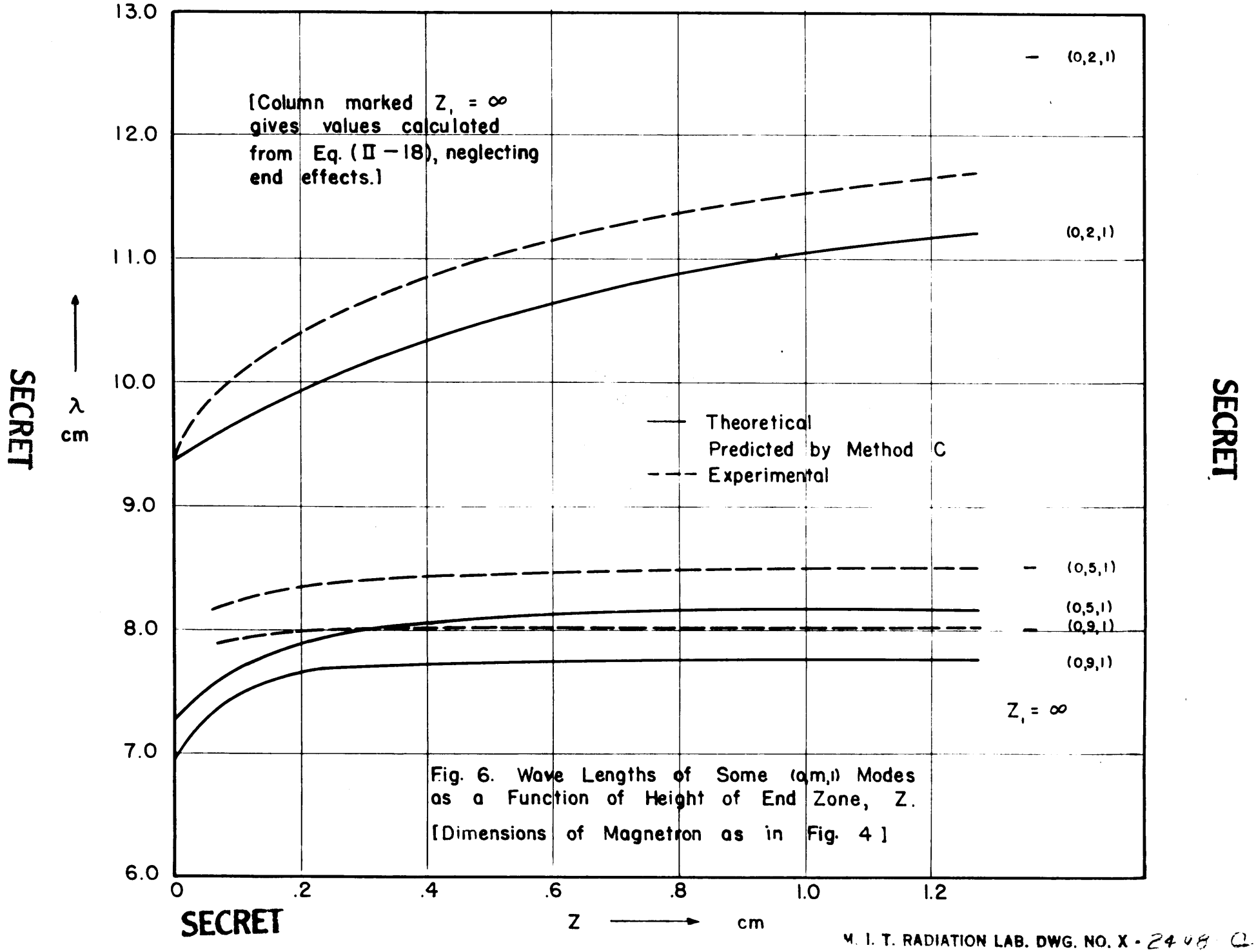

Fig. 6. Wave Lengths of Some (0,m,1) Modes as a Function of Height of End Zone, Z.
[Dimensions of Magnetron as in Fig. 4]

M. I. T. RADIATION LAB. DWG. NO. X - 2408 Q

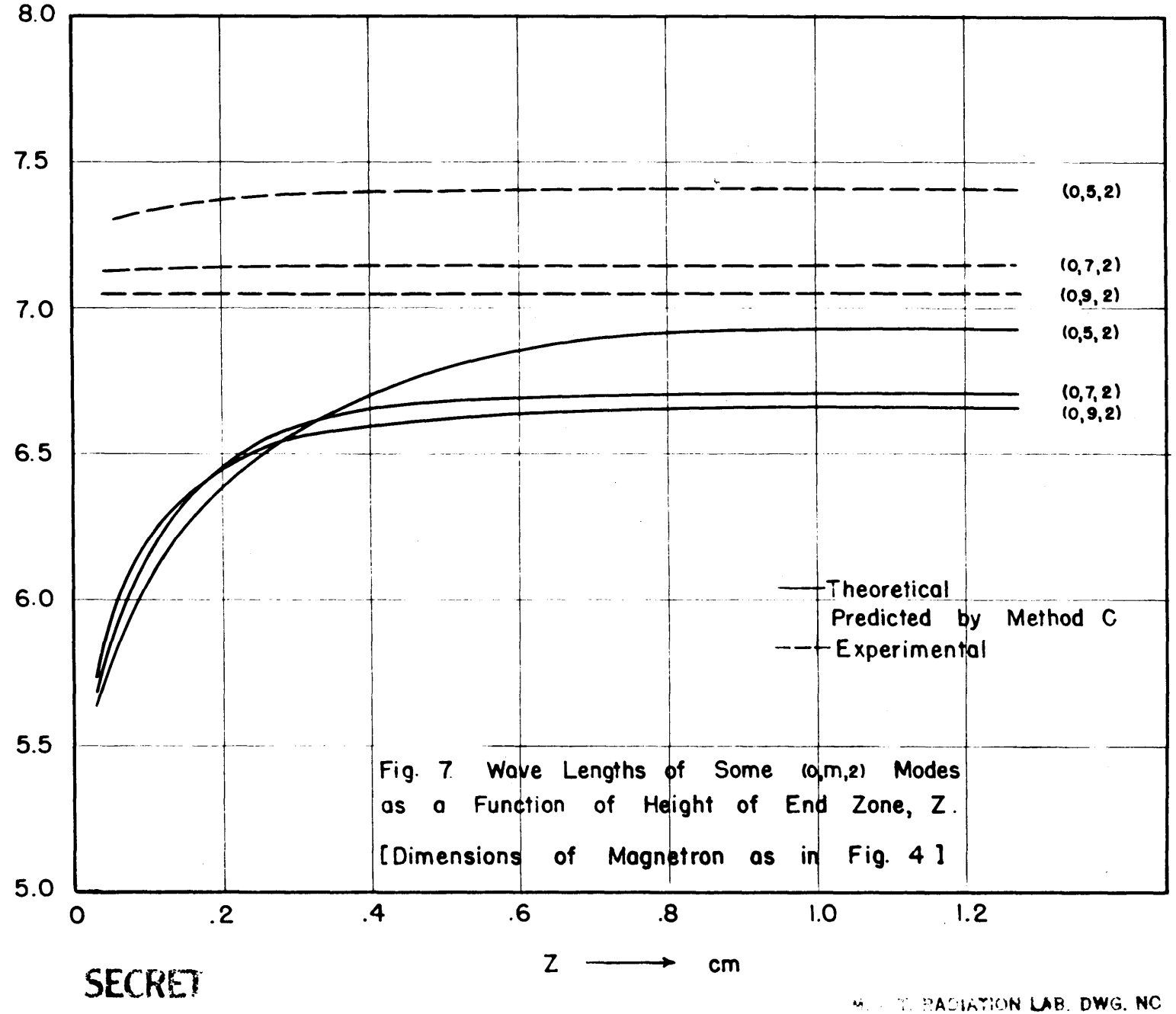

Fig. 7 Wave Lengths of Some (0,m,2) Modes as a Function of Height of End Zone, Z.

[Dimensions of Magnetron as in Fig. 4]

Due to the uncertainty in the 'fringing' corrections the magnitude of the end effect for higher modes is ambiguous. The measured wave lengths even appear to be a trifle higher than those calculated neglecting end effects. At most the end effect for these modes is about 1%. However Eq. (II-30) predicts an effect of more than 3%!

This large discrepancy is not surprising since the calculation completely neglects the higher modes generated near the edges. If we attempt to introduce these higher modes through the field given in Eq. (II-9), the chief change is to replace $\frac{\sin k_{ym} d/2}{k_{ym} d/2}$ by $J_o(k_{ym} d/2)$, which has a negligible effect. But it is evident that this in not a consistent method of taking the higher modes into account. This field corrects only for the effect of the edges at $z = z_1$, and at $x = X$. However the higher modes generated near the edge of the vane at the junction of Regions I and III must have a much larger effect. It is believed that these higher modes arise in the following manner. Eq. (II-6) gives k_x' as a function of k_{yo}. Heretofore only the lowest root of this equation has been used. Due to the periodicity of tan $k_x'L$ higher solutions do exist. They have a variation in the z-direction given by

$$k_z = \sqrt{k^2 - k_x'^2}$$

and k_z is therefore imaginary. These solutions thus are important only near $z = z_1$ and decay rapidly away from these planes.

However there seems to be no simple way of including these higher modes in the calculations, since we have no way of assigning amplitudes to each solution. The problem is complicated as these solutions are not orthogonal in any range. The only feasible method would seem to be a rather laborious variational procedure.

III. Experimental Study of a Linear Magnetron

1. Description of Apparatus

In order to investigate experimentally the effects of the end zones a 10 slot linear magnetron has been constructed, and its resonant modes measured.

Details of the construction are shown in Figs. 8, 9, and 10, and the important dimensions are summarized in Table IV.

Table IV

Dimensions of Linear Magnetron

$L = 1.753 \pm .005$ cm.

$d = .476 \pm .003$ cm.

$Y = .952 \pm .002$ cm.

$X = 1.905 \pm .010$ cm.

$2z_1 = 3.493 \pm .003$ cm.

$Z = 0.0$ to 1.27 cm.

The slots are milled in a brass plate 1" thick fastened to a similar brass plate. This solid base reduces distortions due to strains produced in milling. At each side of the plate the vanes are cut away to form ledges 1/2 " wide. Bolted on to the ends of the plate are 1/2 " brass end-plates, each containing five holes permitting the insertion of loops at various positions. The slots at the ends of the plate are cut half width, so that

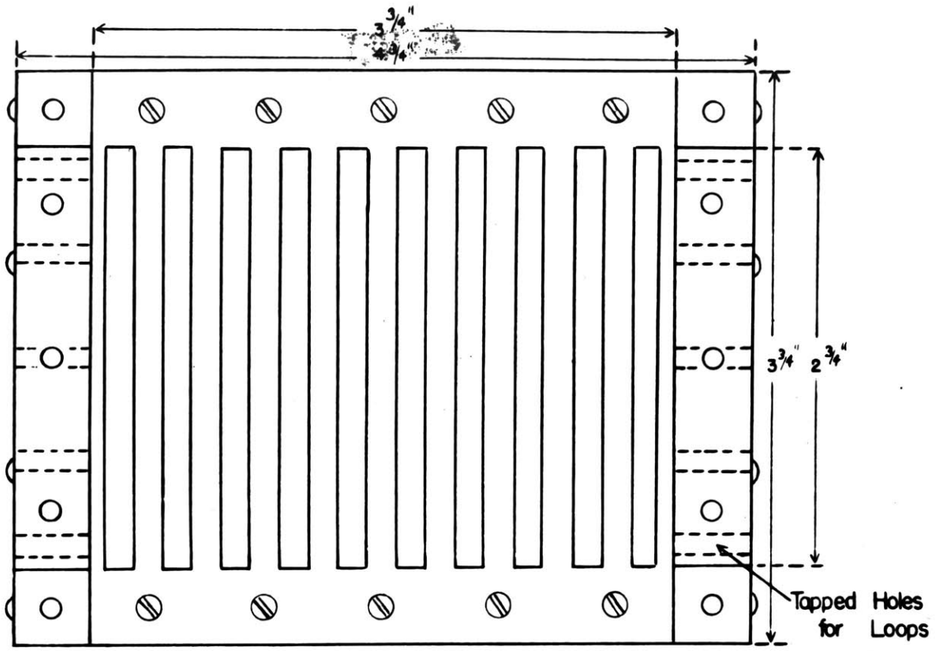

Plan

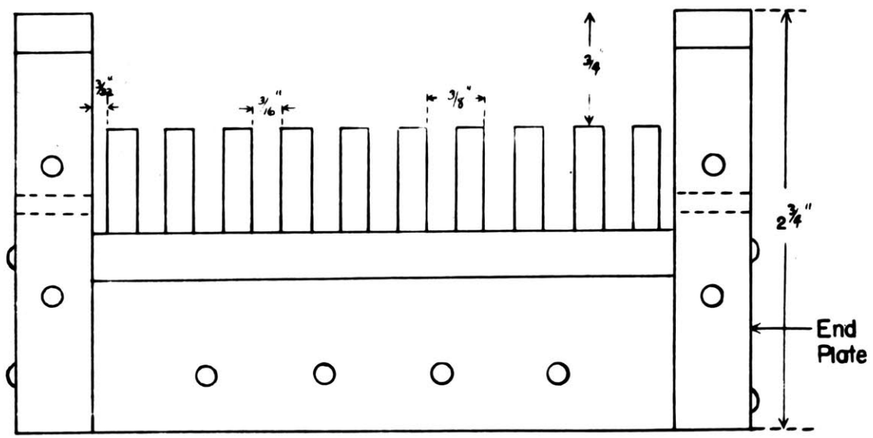

Elevation

a

Fig. 8

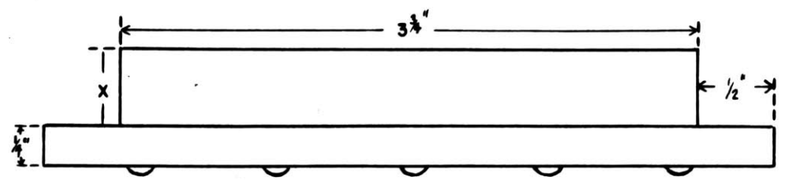

Plan

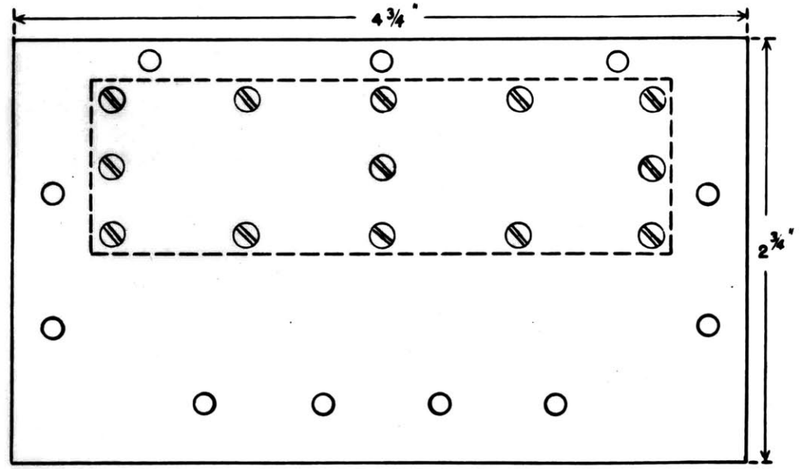

Elevation

Side Plate

b

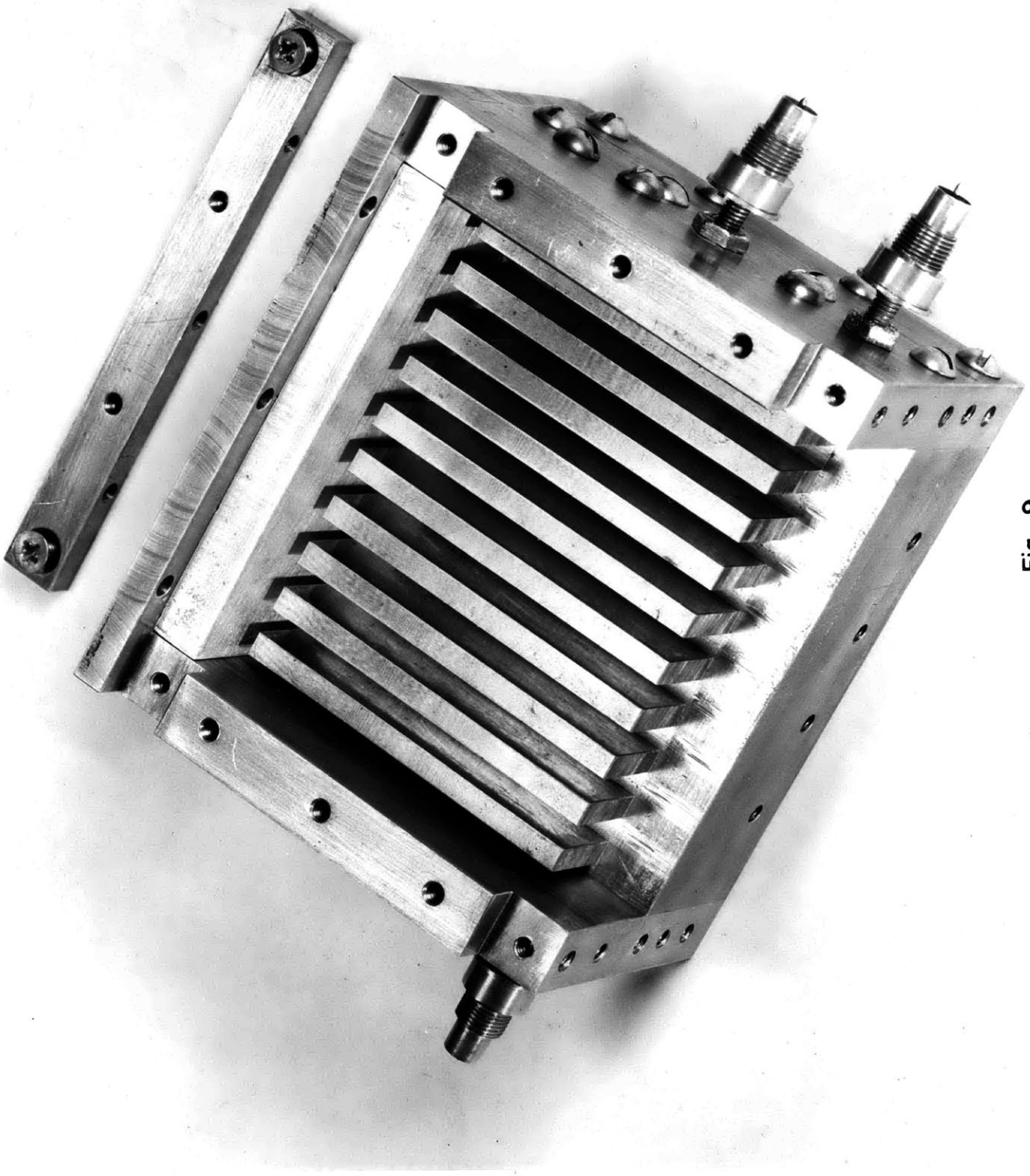

Fig. 9

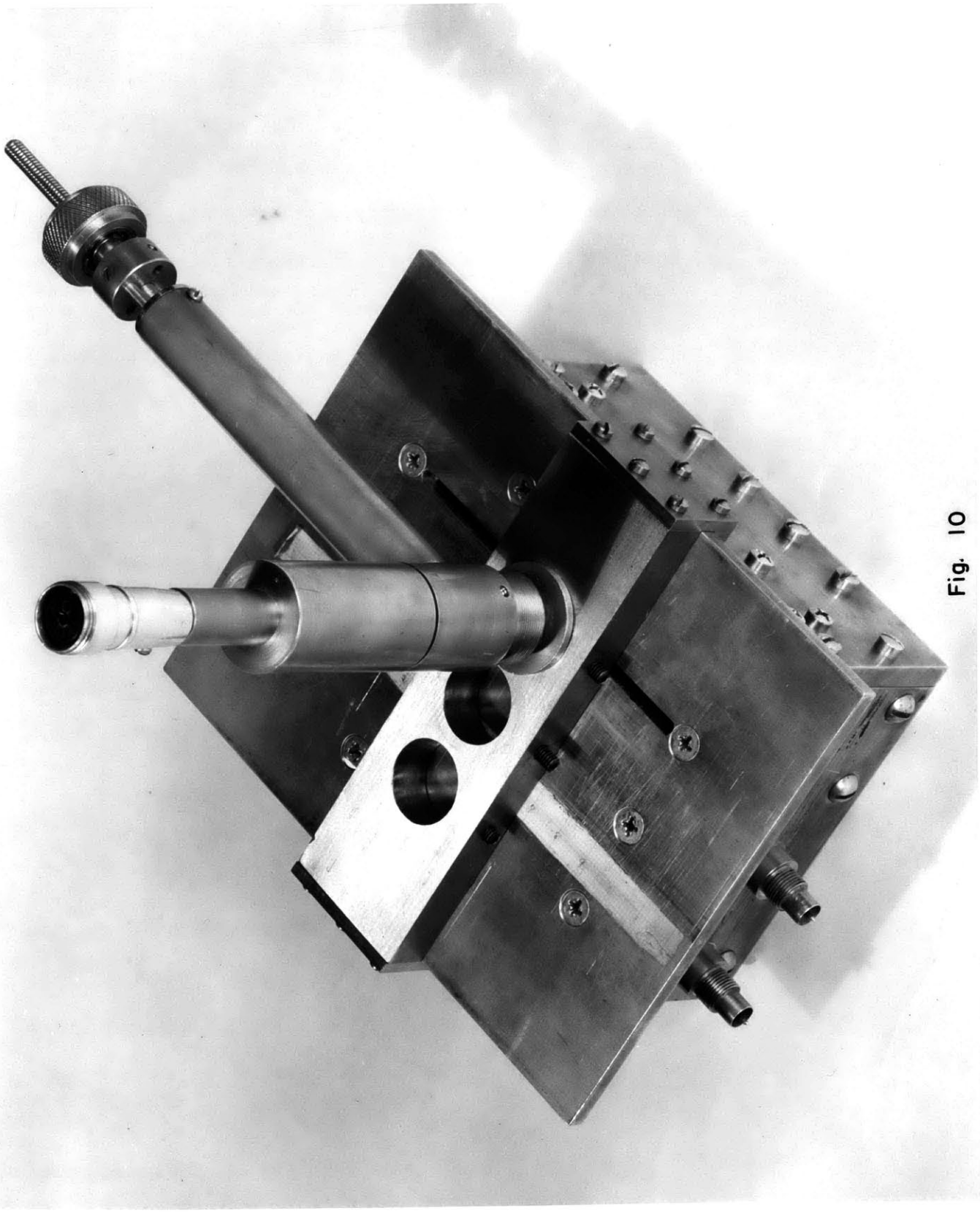

Fig. 10

together with their images in the end plates they constitute slots of normal width. Fitting in notches cut at the top of each end plate are two bars stretching from one plate to the other. These cross bars help to anchor the brass plates which form the sides of the cavity. The side plates carry blocks of varying thickness, as shown in detail in Fig. 8b, which fit rather tightly between the ledge and the cross bar. The spaces between the vanes and the blocks constitute the end zones. The size of the end zone can be changed by varying x, the thickness of the blocks. The positions of these blocks and of the end zones are clearly shown in Fig. 9. It was thus possible to vary Z in eight steps from .013 cm. to 1.27 cm. A slotted cover plate completes the cavity. Two plates were used, one with a slot in the middle, the other with the slot displaced 1" from the center. The standing wave pattern of the fields in cavity was measured by a probe inserted in the slot. The completely assembled linear magnetron (including the probe holder, or carriage, and tunable probe) is shown in Fig. 10.

The experimental arrangement for the measurement of the resonant wave lengths is shown schematically in Fig. 11. In the region from 6.5 cm. to 9.7 cm. a Western Electric 1332 CT (Samuel tube) was used, while the region from 8.7 to 13.0 cm. was covered by a Western Electric 707 A (McNally tube). Various types of probes were tried. The standard non-tunable wave guide probe designed for use at 10 cm. was used, with the bolometer element replaced by a crystal. More sensitive was the tunable 10 cm. probe, kindly lent by Dr. Krutter, shown in Fig. 10. Many of the later measurements were made with a "home made" probe with a double stub

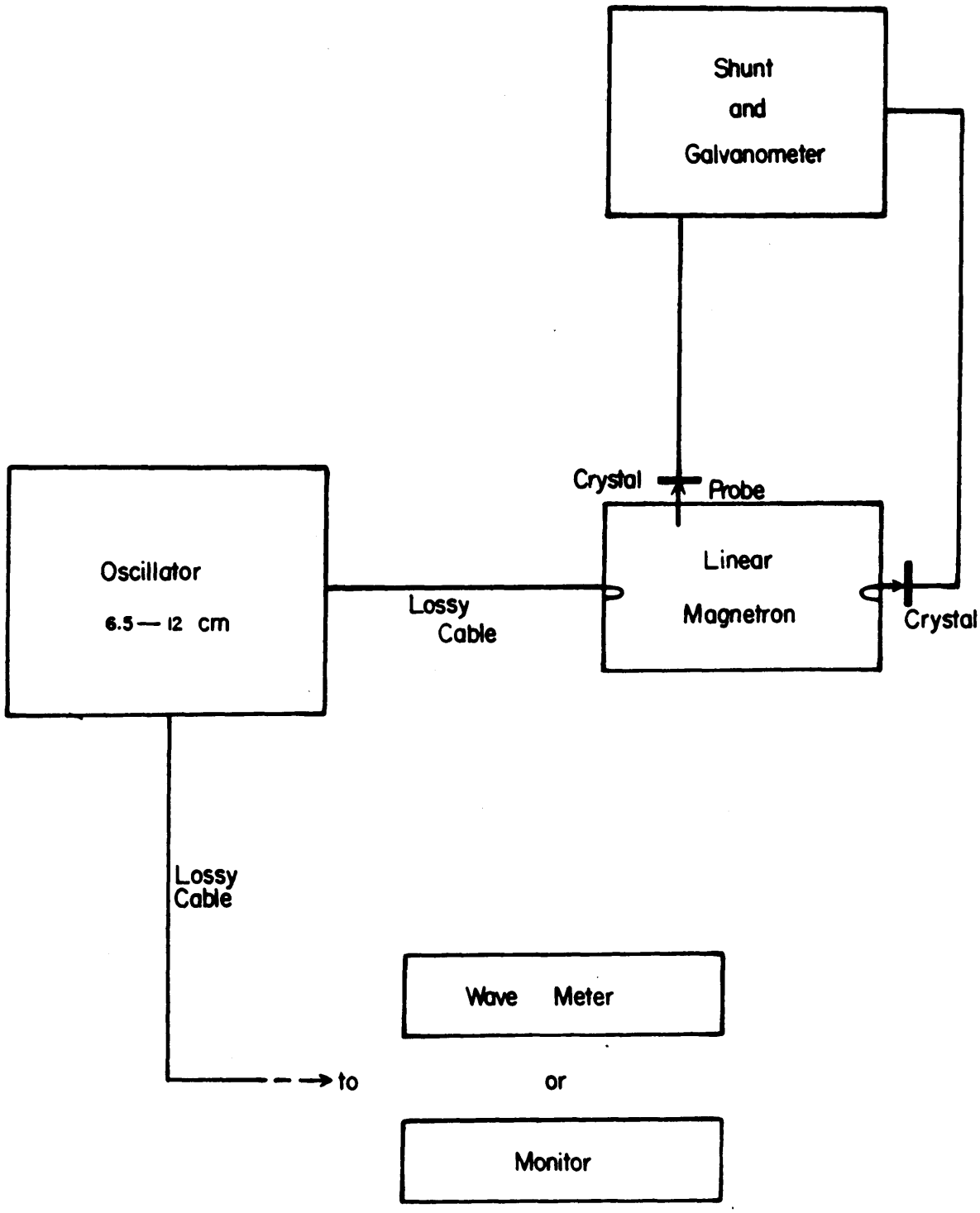

Fig. 11

M. I. T. RADIATION LAB. DWG. NO. X-2385-G

tuner constructed of standard Sperry fittings, which proved most sensitive of all. Wave lengths were measured with a Radiation Laboratory Type 401 open end coaxial wavemeter, which is stated to have an absolute accuracy of .1%. Readings could be reproduced to a much smaller error, about .02 to .03%. The galvanometer used to measure the currents in both the output loop and the probe was a Rubicon galvanometer, sensitivity = 3.0×10^{-9} amp./mm. The greater sensitivity compared to the more customary microammeter was essential for the investigation of the higher modes, since the fields at the probe are very weak.

Several minor changes were often made in the set up shown in Fig. 11. Thus whenever possible the wavemeter and monitor were simultaneously connected to the r.f. line through a reaction coupler, essentially a T-joint. This arrangement, while very convenient, could not be used often as the sensitivity was then greatly reduced.

2. Discussion of Method and Results

The technique of cold resonance measurements has been described by Slater[7], Tonks and Crawford[8] and others, and need be given only briefly. Resonances are detected by means of an output loop, similar to the input loop. The index m of the mode is given by the number of maxima in the standing wave pattern measured by the probe. The (0,m,1) modes are distinguished from the (0,m,2) modes by the difference in the method of excitation. If the input loop is in the center, i. e., in the z = 0 plane (Fig. 3), only the (0,m,1) modes are excited, while if the loop is

---

[7] J. C. Slater, Radiation Laboratory Report 43-9

[8] L. Tonks and S. N. Crawford, General Electric Research Laboratories, report dated 7/15/42

placed off center both the (0,m,1) and (0,m,2) modes are generated. Similarly, when measuring a (0,m,2) mode the slot for the probe, and the output loop must be placed off-center, as shown in Fig. 10. In practice two output loops were used, one in the middle and the other in the outermost hole. If the resonance could not be detected in the center loop, it definitely belonged to a (0,m,2) mode. By these means it was often possible to distinguish a (0,m,2) mode from a nearby (0,m,1) mode even though the two were much closer than the width of the resonance curve.

Energy could be radiated from the slot in the top plate when in the off-center position. This was prevented by a brass plate cut to fit around the probe carriage and so arranged as to cover all of the slot not covered by the probe and its holder.

Beside the slot for the probe the cavity differed from the ideal geometry of Fig. 3 by the presence of the cross bars and loops. The cross bars are in Region IV where the fields are very weak and hence, as Slater[9] has shown, should affect the resonant frequencies only slightly. In one experiment the cross bars were temporarily removed without changing the wave length of the (0,3,1) mode by more than .05%. The loops, each less than .02 cm.^{2} in area, likewise had neglibible effect. Several times the input and output loops were withdrawn until they were practically flush with the wall. The currents decreased by a factor of more than one hundred, but the resonant wave lengths remained unchanged to within .002 cm. The width of the resonance curve was also unaffected. Because the cavity and wavemeter were simultaneously connected to the oscillator little trouble was experienced from 'pulling'.

---

[9] J. C. Slater, Radiation Laboratory Report 43-16

The results are presented graphically in Figs. 12 and 13, and the actual measurements are tabulated in Appendix II. In Fig. 12 the column of dashes marked $z_1 = \infty$ are calculated values assuming the oscillator cavities so long that end effects may be neglected, i. e., $k_z = 0$. The edge effects as corrected by Eq. (II-18) are included in these values. The points marked $Z = \infty$ were experimentally measured by removing the side plates. They differ only slightly from the wave lengths for $Z = 1.27$ cm. The (0,1,1) mode was never found as it must be above the range of the oscillator. The (0,10,1) mode could not be detected and the (0,10,2) mode was found only for $Z = 1.27$ cm. and $Z = \infty$. These modes were apparently so weakly excited that they were often lost in the resonance curve of the neighboring $m = 9$ mode. In the two cases in which the (0,10,2) mode was found, its amplitude was 1/8th of the (0,9,2) mode. Modes whose index n is greater than 2 have wave lengths in general that are outside the range of the oscillator. However, a mode occurring at about 6.9 cm. is believed to be the (0,2,3) mode.

As the result of an error in machining the blocks attached to the side plates did not make contact with the ledge, i. e., with the $x = x + L$ plane. The gap between the two was sometimes as much as .004". To correct the situation the blocks were silverplated to a thickness of .006". They were then too large for the space between the crossbar and the ledge. To insert them the crossbar was loosened slightly, until the block could slip in, and then screwed down tightly. It was hoped in that way to insure contact between the metal surfaces. A conducting grease, "Lubriplate" was also used between the surfaces. The magnetron could be taken apart and reassembled without any noticeable change in the resonant

Fig. 12

Measured Wavelength of Some Modes of a Linear Magnetron, Plotted against Height of End Cavity, Z.

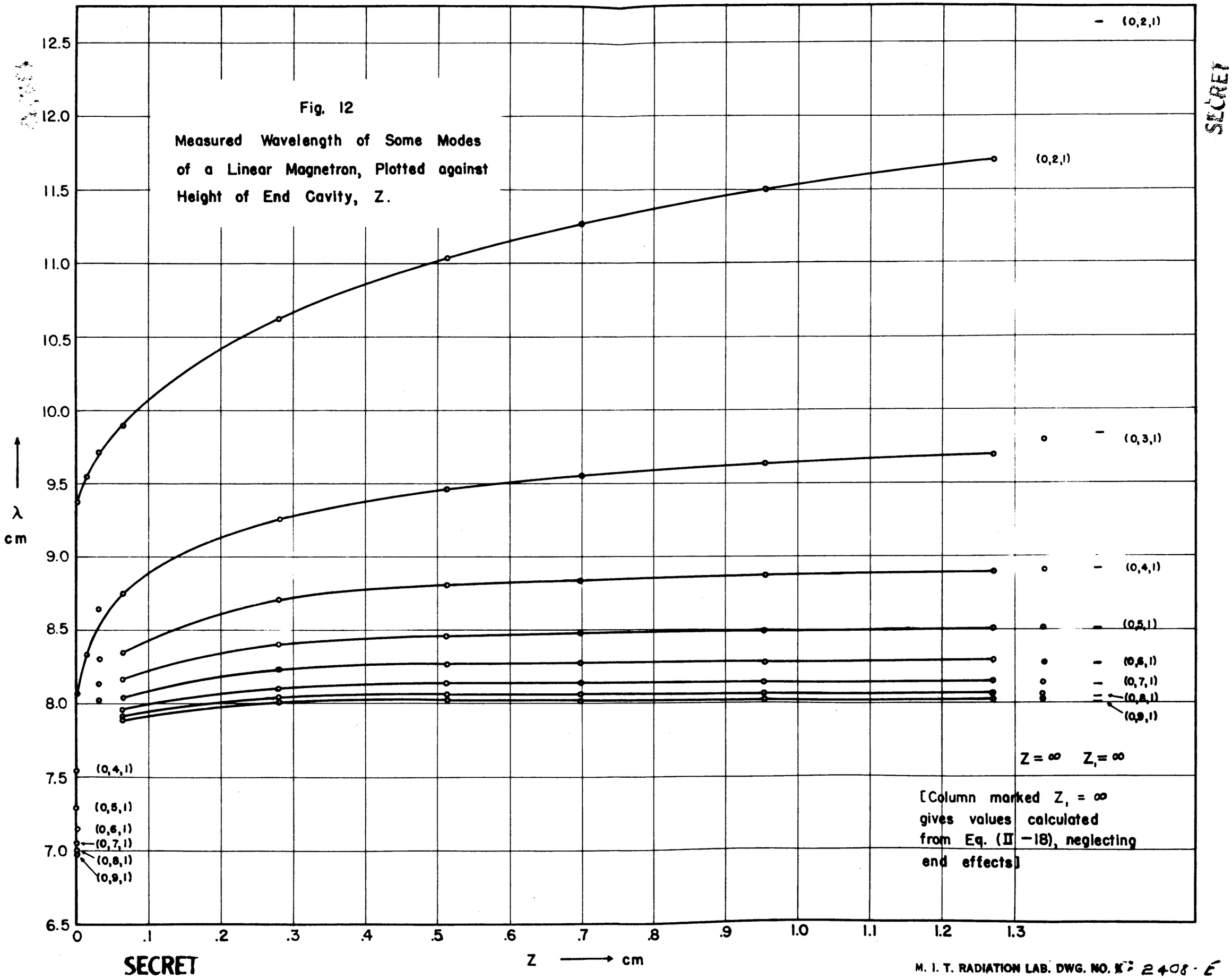

M. I. T. RADIATION LAB. DWG. NO. K- 2408-E

Fig. 13

Measured Wavelength of Some Modes of a Linear Magnetron, Plotted against Height of End Cavity, Z.

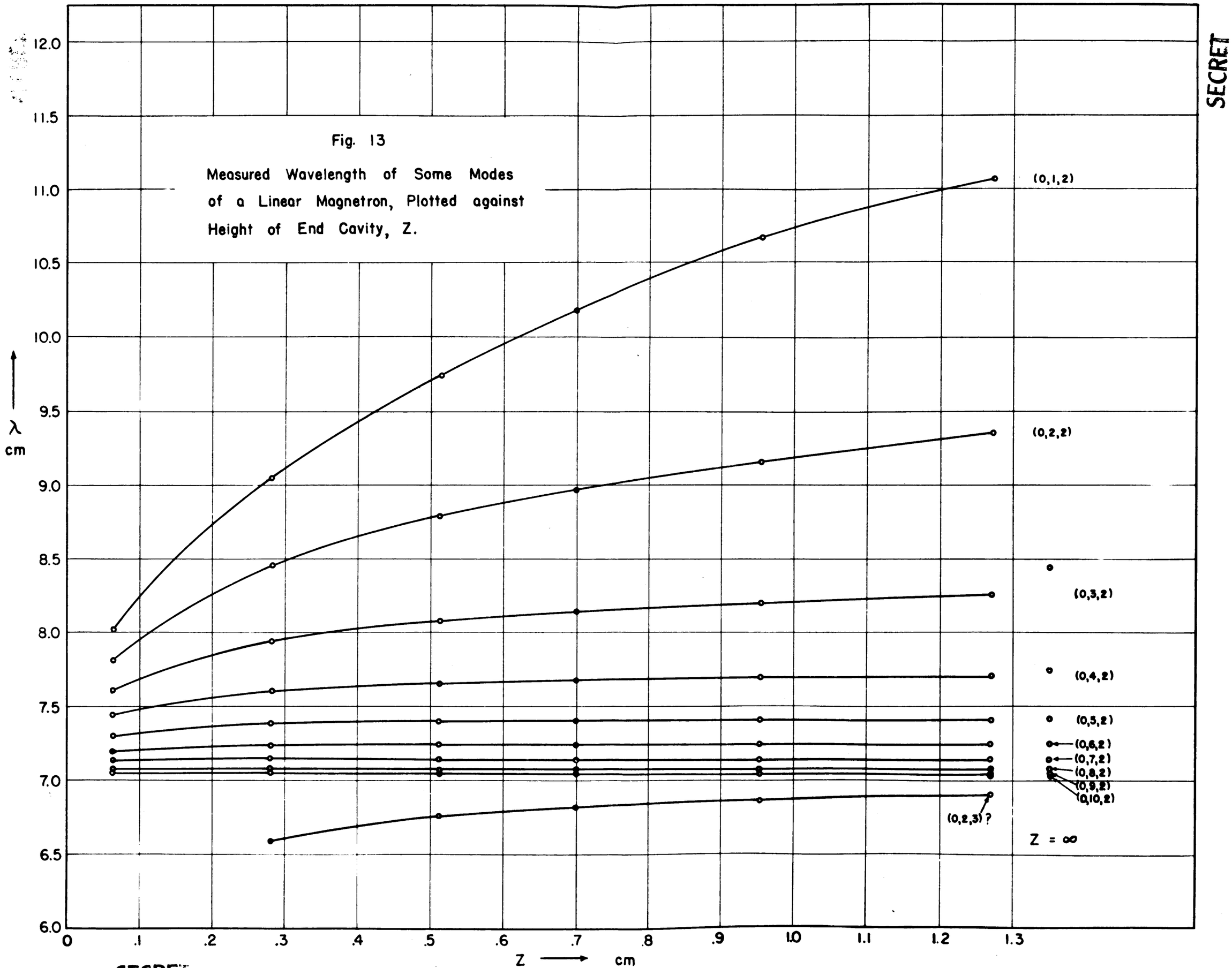

M. I. T. RADIATION LAB. DWG. NO. X-2408-F

frequencies. However the condition of the Lubriplate film showed that the blocks for Z = .030 cm. still did not make contact. It will be noticed that the points for this end zone in Fig. 12 are definitely too high. For Z about .3 cm. and larger the effect of the gap is small, the correct wave length being at worst .6% lower for the (0,1,2) mode than when the gap is present. As Z decreases the error increases to several per cent for (0,m,2) modes at Z = .08 cm. In fact, elimination of the gap changed the qualitative behaviour of the (0,m,2) modes. When the original blocks were used, it appeared that the wave lengths increased as Z became very small. After the blocks were silverplated, it was found that the wave lengths actually decreased slightly, as shown in Fig. 13.

At very small values of Z the measurements became quite difficult. The patterns measured by the probe became unsymmetrical and distorted, and slight differences between the sizes of the end zone on each side destroyed the distinguishing symmetries of the (0,m,1) and (0,m,2) modes. The intensity of the modes also decreased quite rapidly. At Z = .030 cm. few modes were recognizable, while at Z = .013 cm., only the (0,2,1) and (0,3,1) modes could be detected at all. It is unfortunate that measurements could not be made in this region. As far as the measurements went the wave lengths of the higher modes did not seem to change appreciably with Z. However if the wave lengths are to reach their proper limiting values at Z = 0, they must drop sharply at least 1 cm. for a further change of Z of .06 cm. It is possible, therefore, that the modes cross over somewhere in this region.

The limiting values for Z = 0 were measured as follows. With the largest blocks in place the size of the end zone was .007". The screws

fastening the side plates to the magnetron were loosened so that a copper foil .010" thick could be inserted in the gap. The screws were then tightened as much as possible. It is certain that the tops of the vanes were in contact with the copper foil. "Lubriplate" was also applied to all surfaces. In Table V the results for the (0,m,1) modes are given. Also tabulated are the calculated wave lengths found from

$$\lambda = \frac{2\pi}{\sqrt{k_x'^2 + \left(\frac{\pi}{2z_1}\right)^2}} \qquad (III-1)$$

The values in the third column are calculated from k_x' as given by Eq. (II-8), while those in the fourth column are corrected for edge effects as given by Eq. (III-18).

Table V

Resonant Wave Lengths for Z = 0

Mode	Exp.	Theor.(Eq. II-8)	Theor.(Eq. II-18)
0,2,1	9.378 cm.	9.42 cm.	9.37 cm.
0,3,1	8.071	8.09	8.04
0,4,1	7.548	7.57	7.51
0,5,1	7.298	7.31	7.26
0,6,1	7.156	7.16	7.12
0,7,1	7.063	7.07	7.03
0,8,1	7.004	7.019	6.97
0,9,1	6.977	6.992	6.95

The measured wave lengths are somewhat shorter than the theoretical values

found from Eq. (II-8). But they are larger than the values corrected for edge effects, and are often closer to the cruder results. While part of this error is probably of experimental origin, due to imperfect contacts, etc., some of it may be evidence of the 'over correction' mentioned previously. In either case the difference between experiment and theory is never greater than .5%.

3. Measurement of Q.

Because of the many imperfect contacts present the linear magnetron described here is particularly unsuited for measurements of dissipation in the walls. However some rough measurements of the unloaded Q were made in the following manner. The wave lengths λ_1, λ_2 were found for which the galvanometer deflection was just one half of the maximum deflection at the peak of the resonance. The Q is then given by

$$Q = \frac{\lambda_o}{\lambda_2 - \lambda_1} \qquad (III-2)$$

where λ_o is the resonant wave length. As was mentioned before the loading by the loops was negligible. Hence these values of Q should be a measure only of the dissipation in the walls. The method used assumes the resonance to be so narrow that the oscillator output is constant between λ_1 and λ_2, and that the frequency sensitivity of the cables and crystal may be neglected in that band. It also assumes that the oscillator wave length and output remain unchanged during the time required for a measurement, which was not always the case. Further it is supposed that the crystal is a perfect square law detector, which is not true for crystal currents greater than a few microamperes. In addition $\lambda_2 - \lambda_1$ was often not much greater than the error in setting of the wavemeter. Because of these many sources of

inaccuracies the measurements must be considered as only giving the order of magnitude. For large Z the Q values for all modes were scattered between 700 and 1000, the most careful measurements giving a Q of 800 for the (0,7,1) and (0,9,1) modes. The lower modes seemed to have a slightly lower Q. This might be due to radiation from the slot, especially in the (0,m,2) modes, despite the precautions taken. At smaller Z the Q was much less, about 300. This behavior is to be expected as the large magnetic fields in the end zone would increase the dissipation, especially if the contact between the block and the ledge is not good.

Some rough calculations of the unloaded Q have been made and are presented in Appendix III. The computation was made with the following approximations: (1) The energy stored in Regions I and IV and the dissipation in their walls was neglected. (2) In the oscillator cavities it was assumed that there was no variation of the field with z, i.e., $k_z = 0$. (3) The energy of the field in the end zones was neglected, and it was assumed that dissipation in the side walls of the end zones was negligible. The final result is

$$Q = \frac{1}{\delta} \frac{Ld\left[1 + \frac{\sin 2R_x' L}{2R_x' L}\right]}{d + L\left[1 + \frac{\sin 2R_x' L}{2R_x' L}\right] + \frac{2-\delta_{mN}}{2}\frac{L}{\beta_1}\frac{d^2}{Y^2}\left[1 + \frac{\sin 2R_x' L}{2R_x' L}\right]\sum_{\ell=0}^{1} \coth^2 R_{y\ell} Z \left(D + d\,\delta_{mN}\frac{\sin R_{y\ell} d}{R_{y\ell} d}\right)} \qquad \text{(III - 3)}$$

where δ is the skin depth and δ_{mN} is the Kronecker symbol. For Z = 1.27 cm. the calculated Q values, for brass walls, ranged from 1410 for the (0,2,1) mode to 1670 for the (0,9,1) mode. There is thus a factor of two between theory and experiment. Considering the roughness of the surface, the uncertainty as to its actual conductivity, and the many doubtful contacts, the agreement is quite good.

IV. The Corrugated Wave Guide

When the linear magnetron is used as a wave guide, it has the property that the guide wave length, λ_{yo}, is less than the wave length of the $(T.E.)_{1,0}$ mode in a rectangular wave guide of equal width. By a suitable choice of dimensions it is even possible to reduce λ_{yo} below the free space wave length, λ. This property has several applications in the design of antennas consisting of linear arrays. When used in this manner the linear magnetron has been called a "corrugated wave guide". This section discusses the properties of corrugated wave guides, especially attenuation. The limiting case in which the end zones have vanished will be treated first in considerable detail, as the theory there can be developed more accurately than for the general case.

1. Without end zones

The relation between λ_{yo} and the free space wave length can easily be found from the work described in Section II. Either Eq. (II-8) or Eq. (II-18) may be used to determine k_x' in terms of $k_{yo} = \frac{2\pi}{\lambda_{yo}}$, and λ is then given by Eq. (III-1). In Fig. 14 λ_{yo} calculated using Eq. (II-8) is plotted against λ for a corrugated wave guide of typical dimensions. The ordianary cut-off of the wave guide occurs at 4.58 cm., and there is another cut-off arising from the resonance of the slots at 2.10 cm. The wave guide thus acts as a band-pass filter. Also shown are several measured values of λ_{yo}[10] which are about 5% larger than the calculated values. The difference is apparently the result of improper soldering in the construction of the wave guide so that the actual width $2z_1$ is less than the

---

[10] Experiments of Dr. H. Krutter, described in Radiation Laboratory Report 54-16

M. I. T. RADIATION LAB. DWG. NO. X - 2411-A

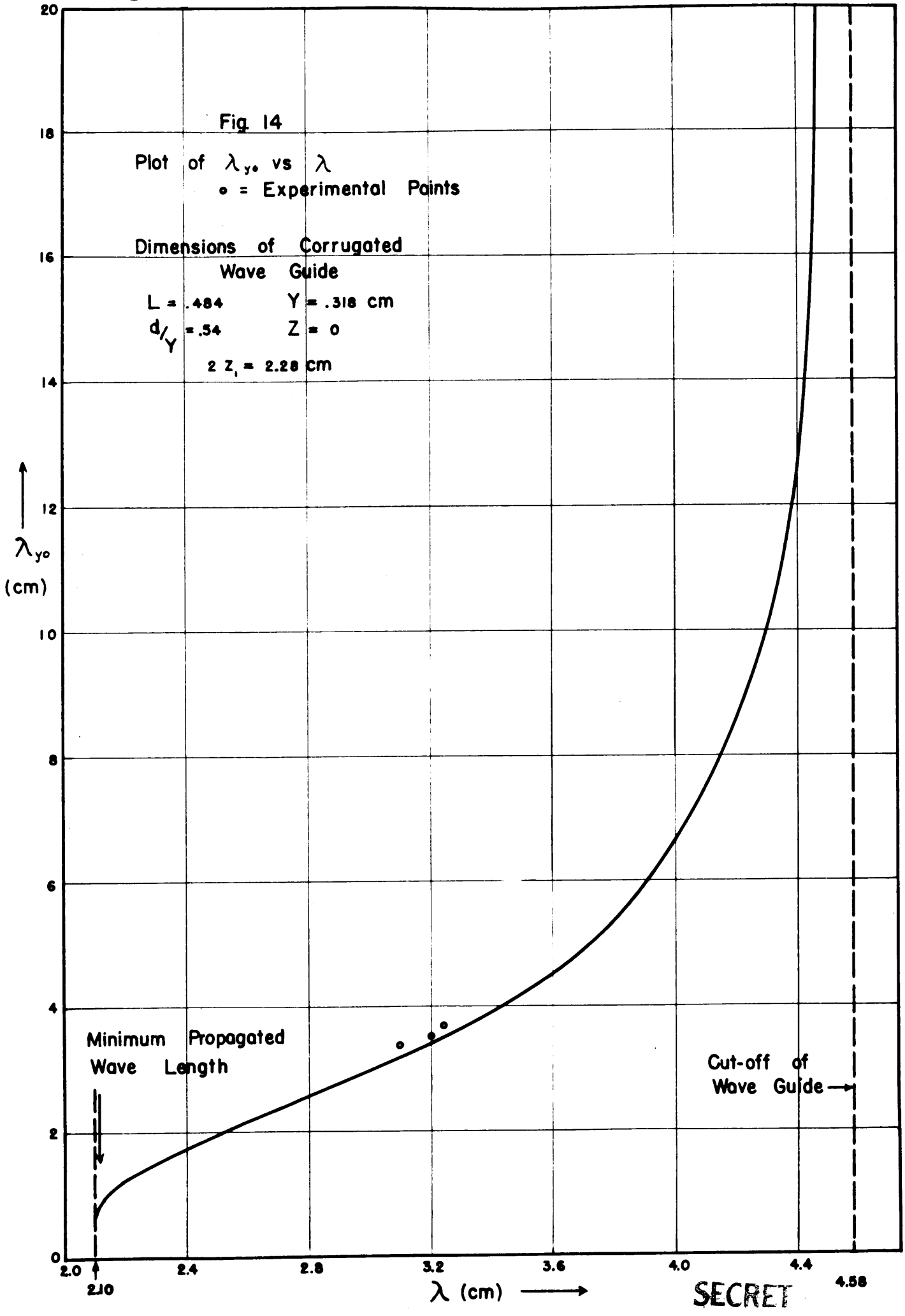

apparent value.

The attenuation due to joulean losses in the metal walls is calculated by considering the finite conductivity to be a small perturbation on the fields found for ideal walls. This method is discussed in detail by Slater[11]. In addition to the assumptions made there it will be assumed that the length of the guide is large compared to Y, the distance between slots. The attenuation of the fields is

$$\alpha = \frac{1}{2} \quad \frac{\text{Power flowing into the metal walls per unit length}}{\text{Power propagated down the guide}}$$

Those components of the fields in Region I that are needed are:

$$\left.\begin{aligned} B_z &= \sum_{-\infty}^{+\infty} a_m e^{i k_{ym} y} \cosh k_{xm} x \cos k_z z \\ B_x &= -\sum a_m \frac{k_{xm} k_z}{k_x'^2} \sinh k_{xm} x \sin k_z z \, e^{i k_{ym} y} \\ B_y &= -\sum a_m \frac{i k_{ym} k_z}{k_x'^2} \cosh k_{xm} x \cos k_z z \, e^{i k_{ym} y} \\ E_x &= -\sum a_m \frac{\omega k_{ym}}{k_x'^2} \cosh k_{xm} x \cos k_z z \, e^{i k_{ym} y} \end{aligned}\right\} \quad (\text{IV}-1)$$

where $k_z = \pi/2z_1$. In the oscillator cavities the fields generated near the edges of the slot will be neglected. The field components in the jth slot then are:

$$\left.\begin{aligned} B_{xj} &= b_o e^{i k_{yoj} Y} \sin k_x' (x - X - L) \sin k_z z \\ B_{zj} &= \frac{k_x'}{k_z} b_o e^{i k_{yoj} Y} \cos k_x' (x - X - L) \cos k_z z \\ E_{yj} &= \frac{i\omega}{k_z} b_o e^{i k_{yoj} Y} \sin k_x' (x - X - L) \cos k_z z \end{aligned}\right\} \quad (\text{IV}-2)$$

---

(11) J. C. Slater, "Microwave Transmission," McGraw Hill, New York, 1942, P. 138

The time average of the power propagated down the guide is given by

$$\overline{S}_p = Re \int_{-z_1}^{+z_1} \int_0^X \mathcal{S}_y \, dx \, dz \qquad (IV-3)$$

where $\mathcal{S}$ is the complex Poynting vector $\frac{1}{2} E \times H^*$. In terms of the fields given above s_y is:

$$\mathcal{S}_y = \frac{1}{2\mu} \sum_{m=-\infty}^{+\infty} a_m^2 \frac{\omega k_{ym}}{k_x'^2} \cosh^2 k_{xm} x \cos^2 k_z z \qquad (IV-4)$$

$$+ \frac{1}{2\mu} \sum_m \sum_{\substack{l \\ l \neq m}} a_m a_l^* \frac{\omega k_{ym}}{k_x'^2} \cosh k_{xm} x \cosh k_{xl} x \cos^2 k_z z \, e^{2\pi i \frac{m-l}{Y} y}$$

The y dependence of s_y arises from the approximate nature of the matching between Regions I and II. Since B_z is matched only in the average, there exists a component of the Poynting vector in the x-direction corresponding to energy flow into the slot. Averaged over the slot width this component vanishes, and there is no net change in s_y in going from one slot to the next. To eliminate the y dependence we can therefore average s_y over the distance between slots. The value of Eq. (IV-3) is then

$$\overline{S}_p = \frac{z_1 X}{4\mu} \sum_{-\infty}^{+\infty} a_m^2 \frac{\omega k_{ym}}{k_x'^2} \left(1 + \frac{\sinh 2 k_{xm} X}{2 k_{xm} X} \right) \qquad (IV-5)$$

This may be simplified for several cases of interest. When k_{yo} is much less than π/Y the only appreciable term in Eq. (IV-5) is for m = 0. Retaining this term only, and using the value of a_m given by Eq. (II-27) and the approximate relation between k_{yo} and k_x', Eq. (II-8) P. 26, Eq. (IV-5) then reduces to

$$\overline{S}_p = \frac{z_1 X}{4\mu} b_o \frac{\omega k_{yo}}{k_z^2} \left(\frac{\cos k_x' L}{\cosh k_{xo} X} \right)^2 \left[1 + \frac{\sinh 2 k_{xo} X}{2 k_{xo} X} \right] \qquad (IV-6)$$

When k_{yo} is almost π/Y the waves reflected from the slots become important, and for $k_{yo} = \pi/Y$ they are equal to the incident waves, so that there is no net transmission of power. Hence for $k_{yo} \simeq \pi/Y$ both the m = 0 and m = -1 terms in Eq. (IV-5) must be retained. They can be considerably simplified by using the following approximations. If $\delta = \pi/Y - k_{yo}$, then $k_{xo} \simeq \pi/Y - \delta$, $k_{y-1} = -\frac{\pi}{Y} - \delta$, $k_{x-1} \simeq \frac{\pi}{Y} + \delta$. Further, k_x' is almost equal to $\frac{\pi}{2L}$ and therefore sin $k_x'L$ may be replaced by 1. Since $\frac{d}{Y}$ is usually small, $\frac{\sin k_{yo}\frac{d}{2}}{k_{yo}\, d/2}$ can be set equal to 1 too. The two terms then become:

$$\overline{S}_p = \frac{\beta_1}{2\mu} b_o^2 \frac{d^2}{Y^2} \frac{\omega}{K_z^2} \frac{K_x'^2 \delta}{(\pi/Y)^3}, \qquad K_{yo} \simeq \frac{\pi}{Y} \qquad (IV-7)$$

The average rate of energy flow into the metal walls is given by

$$\overline{S}_d = \int s_n \, dA = \frac{1}{2\mu^2}\sqrt{\frac{\mu\omega}{2\sigma}} \int B_t^2 \, dA \qquad (IV-8)$$

where the integrals are to be evaluated over the surface of the metal, and where B_t is the tangential component of the magnetic field. The conductivity of the metal is designated by σ. It is convenient to separate the attenuation α in two parts α_{II}, due to dissipation in the walls of the slots, and α_I due to dissipation in the walls of Region I. Considering α_{II} first, the rate of energy loss in the slot walls, per slot, is:

$$\overline{S}_d(II) = \frac{K_x'^2}{K_z^2} \frac{\beta_1}{2} \frac{b_o^2}{\mu^2} \sqrt{\frac{\mu\omega}{2\sigma}} \left\{ L\left[\left(1 + \frac{K_z^2}{K_x'^2}\right) + \left(1 - \frac{K_z^2}{K_x'^2}\right) \frac{\sin 2K_x'L}{2K_x'L}\right] \right.$$

$$\left. + d + \frac{d}{\beta_1} \frac{K_z^2}{K_x'^2} L\left[1 - \frac{\sin 2K_x'L}{2K_x'L}\right] \right\} \qquad (IV-9)$$

The first term in the parenthesis represents losses in the planes $y' = \pm \frac{d}{2}$; the second term, losses in the plane x = X + L, and the third term, those in the planes $z = \pm z_1$. Using the relation $\omega/\mu = \frac{k}{\mu}\sqrt{\mu/\varepsilon}$, the attenuation α_{II}

can be written as follows for $k_{yo} \ll \pi/Y$:

$$\alpha_{II} = N\sqrt{\frac{\epsilon\omega}{2\sigma}} \quad \frac{d + L\left\{(1+\eta) + \frac{\sin 2k_x' L}{2k_x' L}(1-\eta)\right\}}{\frac{k k_{yo}}{k_x'^2} X \left(\frac{\cos k_x' L}{\cosh k_{xo} X}\right)^2 \left[1 + \frac{\sinh 2k_{xo} X}{2k_{xo} X}\right]} \qquad (IV-10)$$

where $\eta = (1 + \frac{d}{2z_1})\frac{k_z^2}{k'^2}$, $k_z = \frac{\pi}{2z_1}$, and N is the number of slots per unit length. When k_{yo} is almost equal to $\frac{\pi}{Y}$, α_{II} may be written differently:

$$\alpha_{II} = N\sqrt{\frac{\epsilon\omega}{2\sigma}} \quad \frac{d + L\left\{(1+\eta) + \frac{\sin 2k_x' L}{2k_x' L}(1-\eta)\right\}}{2\left(\frac{d}{Y}\right)^2 \frac{k\delta}{(\pi/Y)^3}} \qquad (IV-11)$$

When $k_{yo} - \frac{\pi}{Y}$ is small the magnetic field in the slots is very large compared to the magnetic field in Region I, and α_I can then be neglected in comparison to α_{II}. However, when k_{yo} is small, this is no longer true; in fact, α_I becomes infinite at the cut-off $k_{yo} = 0$. Therefore α_I will be calculated only for small k_{yo}. Using only the first term in the series for the fields the average rate of energy flow per slot into the planes $z = \pm z_1$, in Region I is:

$$\overline{S}_d(z_1) = \frac{1}{2\mu^2} a_o^2 \frac{k_z^2}{k_x'^2}\sqrt{\frac{\mu\omega}{2\sigma}} X Y\left\{1 + \frac{k_{yo}^2 + k_{xo}^2}{k_x'^2} \frac{\sinh 2k_{xo} X}{2k_{xo} X}\right\} \qquad (IV-12)$$

The similar quantity arising from dissipation in the wall at x = 0 is

$$\overline{S}_d(0) = \frac{1}{2\mu^2} a_o^2 \sqrt{\frac{\mu\omega}{2\sigma}} Y z_1 \left\{1 + \frac{k_z^2 k_{yo}^2}{k_x'^4}\right\} \qquad (IV-13)$$

and the dissipation in the face of each vane at x = X is given by:

$$\overline{S}_d(X) = \frac{1}{2\mu^2} a_o^2 \sqrt{\frac{\mu\omega}{2\sigma}} D z_1 \cosh^2 k_{xo} X \left\{1 + \frac{k_z^2 k_{yo}^2}{k_x'^4}\right\} \qquad (IV-14)$$

Combining Eqs. (IV-12), (IV-13), and (IV-14) to give the total dissipation in I, and using only the first term of $\bar{S}_p$, Eq. (IV-5), α_I becomes:

$$\alpha_I = N\sqrt{\frac{\epsilon\omega}{2\sigma}}\;\frac{XY\left\{1+\frac{k_{yo}^2+k_{xo}^2}{k_x^2}\;\frac{\sinh 2k_{xo}X}{2k_{xo}X}\right\}+\left(1+\frac{k_z^2k_{yo}^2}{k_x'^4}\right)\left\{Y_{z_1}+D_{z_1}\cosh^2 k_{xo}X\right\}}{z_1X\;\frac{kk_{yo}}{k_x'^2}\left\{1+\frac{\sinh 2k_{xo}X}{2k_{xo}X}\right\}} \qquad (IV\text{-}15)$$

The attenuation of the energy flow in the guide is often of greater interest than the field attenuation. Expressed in db per meter this attenuation is given by

$$\alpha' = 8.686\,\alpha \;{}^{db}/_{m}.$$

For the dimensions specified in Fig. 14 α' has been calculated throughout the entire range of k_{yo}, using appropriate forms of α_{II} and α_I, and is plotted in Fig. 15 as a function of free space wave length λ. The attenuation goes to infinity at the guide cut-off, and passes through a flat minimum at about $\lambda = 3.60$ cm. As λ decreases still further, the attenuation increases, becoming infinite again at $k_{yo} = \frac{\pi}{Y}$. The attenuation at $\lambda = 3.20$ cm. as measured by Dr. Krutter is 3.3 db/m, compared to the calculated value of .8 db/m. Some of this discrepancy is no doubt due to the approximate nature of the fields used, which is of greater importance here than in the calculation of wave length. It cannot account for all of the difference, since if the edges are rounded off, thus radically changing the fields at the slot edges, there is little decrease in the measured attenuation. Probably improper soldering is the cause of the larger part of this difference, since slight changes in the soldering technique in the construction were enough to increase the attenuation by 4 or 5 db/m.

2. End zones present.

If the corrugated wave guide has large end zones the guide wave length,

SECRET

M. I. T. RADIATION LAB. DWG. NO. X-2411-B

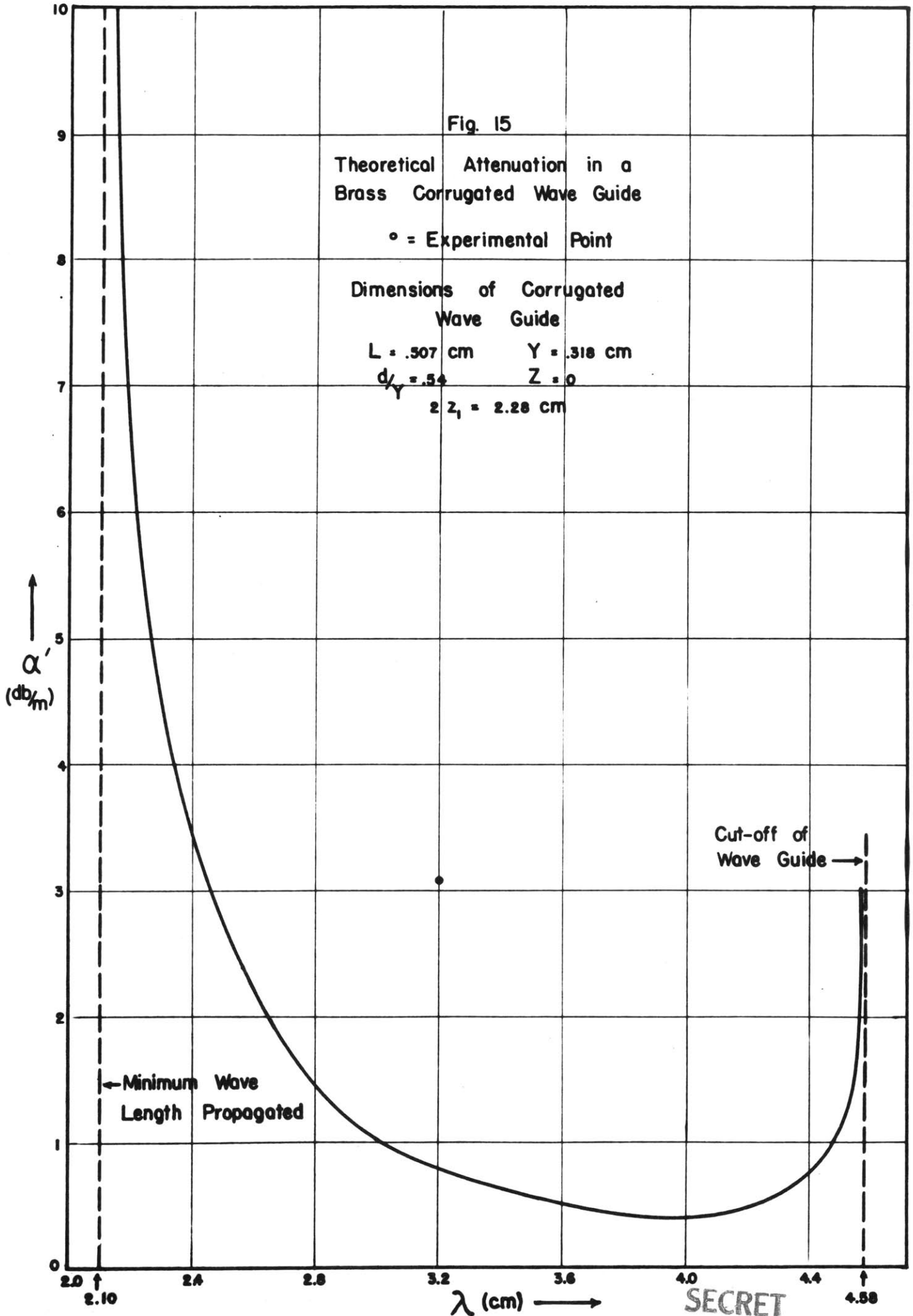

SECRET

λ_{yo}, is much smaller, for the same input frequency, than in a similar wave guide without end zones. This type of wave guide is therefore of greater interest practically than the simpler case. Since the calculation of the effects of the end zones presented in Section II is not accurate, it is not profitable to develop the theory of this case in as great detail as when the end zones are absent.

The guide wave length can be found by using the formulas of Section II, Eqs. (II-8) and (II-32), with about the same accuracy as for the linear magnetron cavity. In Table VI the values measured by Dr. Krutter[12] for two corrugated wave guides are presented.

Table VI

Wave Lengths for Guides with End Zones

Z	λ	λ_{yo}(exp.)	λ_{yo}(calc.)
.08 cm.	3.20 cm.	2.88 cm.	3.04 cm.
.478 cm.	3.20 cm.	2.40 cm.	2.51 cm.

The error in each case is about 5%.

The inaccuracy in the fields should have an even larger effect on the attenuation than on the wave length. For that reason the attenuation will be calculated only roughly, and only for the region of practical interest, i.e., when $k_{yo} < \pi/Y$. Eqs. (IV-2) and (IV-3) can still be used

---

[12] Radiation Laboratory Report 54-16, Table II, Nos. 20 and 22

except that k_z is no longer $\frac{\pi}{2z_1}$. The field components in III which are needed are:

$$\left.\begin{aligned}
B_x &= \sum_{-\infty}^{+\infty} c_m e^{i k_{ym} y} \cosh k''_{zm} (z - z_2) \sin k'_x (x - X - L) \\
B_y &= \sum \frac{i k_{ym} k'_x}{k_z^2} c_m e^{i k_{ym} y} \cosh k''_{zm} (z - z_2) \cos k'_x (x - X - L) \\
B_z &= \sum \frac{k''_{zm} k'_x}{k_z^2} c_m e^{i k_{ym} y} \sinh k''_{zm} (z - z_2) \cos k'_x (x - X - L) \\
E_z &= \sum \frac{\omega k_{ym}}{k_z^2} c_m e^{i k_{ym} y} \cosh k''_{zm} (z - z_2) \sin k'_x (x - X - L)
\end{aligned}\right\} \quad (IV-17)$$

where c_m is given in terms of b_o by Eq. (II-27). The effect of the end zones is small, as has been shown in Sections II and III, and therefore k_z is small. The energy flow in the y-direction in the end zones is proportional to $B_x E_z$, and since B_x is small this energy flow is negligible compared to the power transmitted in Region I. Likewise in calculating the dissipation in the slot walls B_x may be neglected since the ratio B_x/B_z is $\frac{k_z}{k_x}$ tan $k_z z$, which is quite small. The attenuation due to losses in the slots then reduces to:

$$\alpha_{II} = N \sqrt{\frac{\epsilon \omega}{2\sigma}} \; \frac{d + L \left(1 + \frac{\sin 2 k'_x L}{2 k'_x L}\right)}{X \frac{k k_{yo}}{k'^2_x} \left(\frac{\cos k'_x L}{\cosh k_{xo} X}\right)^2 \left(1 + \frac{\sinh 2 k_{xo} X}{2 k_{xo} X}\right)} \quad (IV-18)$$

Similarly in Region I, B_y can be neglected compared to B_z, at least if the wave guide is not operated too near cut-off, and α_I becomes:

$$\alpha_I = N \sqrt{\frac{\epsilon \omega}{2\sigma}} \; \frac{Y + D \cosh^2 k_{xo} X}{X \frac{k k_{yo}}{k'^2_x} \left(1 + \frac{\sinh 2 k_{xo} X}{2 k_{xo} X}\right)} \quad (IV-19)$$

Besides α_I and α_{II} there must now be included the dissipation in the walls of the end zone. Several approximations will be used in the calculation.

We can neglect B_z compared to B_y since the ratio B_z/B_y is approximately $\tanh k''_{z0} Z$ which is small in practice. Since k_z is small, k''_{z0} may be replaced by k_{yo}. Using the relation between c_o and a_o given in Eq. (II-29) the rate of energy loss in the walls of both end zones per slot is found to be:

$$\overline{S_d}(III) = \frac{1}{2\mu^2}\sqrt{\frac{\mu\omega}{2\sigma}}\;\frac{k_{xo}^2}{k_x'^2}\;\frac{\sinh^2 k_{xo}X}{\sin^2 k_x' L}\;\frac{\cos^2 k_z g_1}{\sinh^2 k''_{zo} Z} \cdot \left\{ZY\left(1+\frac{\cosh 2k_{yo}Z}{2k_{yo}Z}\right)+LY+LD\cosh^2 k_{yo}Z\right\} \qquad (IV-20)$$

The attenuation is then:

$$\alpha_{III} = N\sqrt{\frac{\epsilon\omega}{2\sigma}}\;\frac{\frac{\cos^2 k_z g_1}{\sinh^2 k_{yo}Z}\left(ZY\left(1+\frac{\cosh 2k_{yo}Z}{2k_{yo}Z}\right)+LY+LD\cosh^2 k_{yo}Z\right)}{g_1 X\,\frac{k_{yo}k}{k_{xo}^2}\,\frac{\sin^2 k_x' L}{\sinh^2 k_{xo}X}\left(1+\frac{\sinh 2k_{xo}X}{2k_{xo}X}\right)\left(1+\frac{\sin 2k_z g_1}{2k_z g_1}\right)} \qquad (IV-21)$$

Eq. (IV-21) is not valid when Z is small, but roughly it states that the attenuation increases as $1/Z^2$ as Z becomes very small. This is due to a phenomenon which has been qualitatively described previously. Even for small Z, k_z is quite small so that the flux of B_y in the end zones is never less than the flux of B_z in the slots. Hence the magnetic field, and consequently the attenuation, becomes very large. It is for this reason that some corrugated wave guides constructed with very narrow end zones have been found by Dr. Krutter to have abnormally large attenuations.

The total attenuation α', combining Eqs. (IV-18), (IV-19), and (IV-21), has been calculated for the corrugated wave guides of Table VI. With Z = .08 cm. the calculated α' is 1.13 db/m; while the measured value is approximately 12 db/m. For Z = .475 cm. the calculated value is .96 db/m., measured 3.1 db/m. The large discrepancy is probably due to the same reasons as for Case 1, especially for the guide with the narrower end zone. However, the great inaccuracies in the fields contribute a large share of the difference.

V. The Corrugated Coaxial Line

Another device in which the wave length in the line is shorter than the free space wave length is the corrugated coaxial line, shown schematically in Fig. 16. The slots cut in the inner conductor fulfill the same function as the slots of the corrugated wave guide. This section presents a theoretical discussion of the wave length and attenuation in such a line, first, when the slots are empty, and secondly when they are filled with a dielectric.

Case 1. Slots Empty.

As in the previous section effects due to fringing of the field at the slot edges are neglected. The field components in the jth slot are then:

$$\left.\begin{aligned} E_{yj} &= a_o e^{ik_{yoj}Y} C_o(k, r, r_j) \\ B_{\theta j} &= -\frac{ik}{\omega} a_o e^{ik_{yoj}Y} C_{1,o}(k, r, r_j) \end{aligned}\right\} \quad (V-1)$$

where the y-direction is along the axis of the line. The fields in the region outside the slots are chosen transverse magnetic to the y-direction. The y dependence of E_y in that region is $e^{ik_{ym}y}$, while the r dependence, R(r), is given by the Bessel equation:

$$r^2 \frac{d^2R}{dr^2} + r \frac{dR}{dr} + (k^2 - k_{ym}^2) r^2 R = 0 \qquad (V-2)$$

Since k_{ym} is always larger than k, appropriate solutions of this equation are modified Bessel functions $I_o(k_r r)$ and $K_o(k_{rm} r)$, where $k_{rm} = \sqrt{k_{ym}^2 - k^2}$. Instead of $K_n(k_{rm} r)$, it will be more convenient to use the functions $L_n(k_{rm} r) = e^{-\pi n i} K_n(k_{rm} r)$, which obey the same recurrence relations as

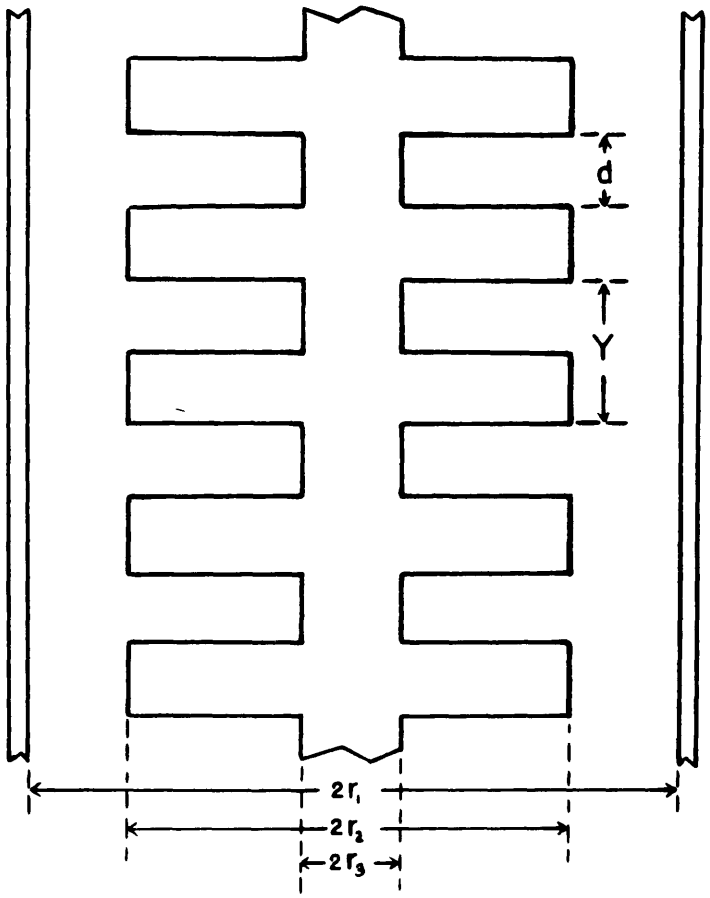

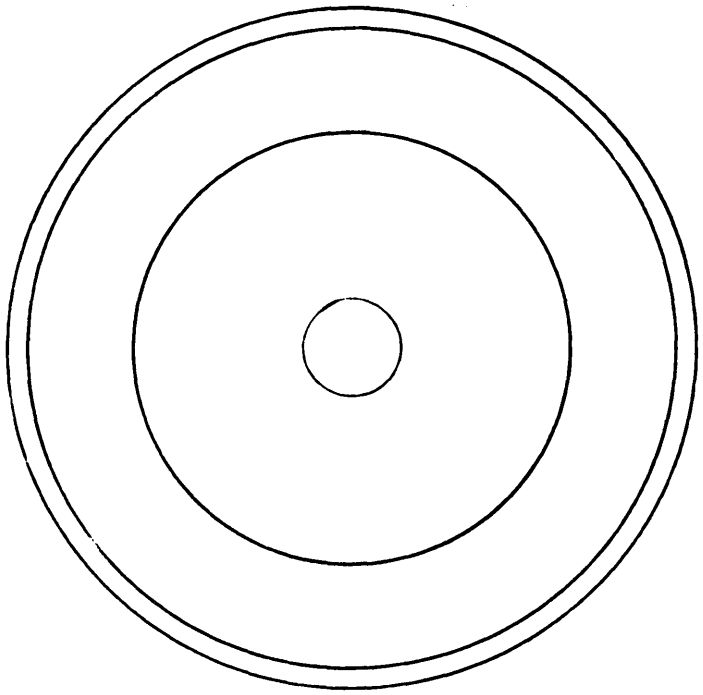

Fig. 16

$I_n(k_{rm}r)$. The fields in this region can then be written as:

$$\left.\begin{aligned} E_y &= \sum_{-\infty}^{+\infty} b_m F_o(k_{rm}, r, r_1)\, e^{ik_{ym}y} \\ B_\theta &= -\sum \frac{ik^2}{\omega k_{rm}} b_m F_{1,o}(k_{rm}, r, r_1)\, e^{ik_{ym}y} \\ E_r &= -\sum \frac{ik_{ym}}{k_{rm}} b_m F_{1,o}(k_{rm}, r, r_1)\, e^{ik_{ym}y}, \end{aligned}\right\} \quad (V-3)$$

$$k_{ym} = k_{yo} + \frac{\pi}{Y}$$

where the functions F_n, $F_{n,j}$ may be termed modified cylinder functions and are defined as:

$$\left.\begin{aligned} F_n(k_{rm}, r, r_1) &= I_n(k_{rm}r)L_n(k_{rm}r_1) - L_n(k_{rm}r)I_n(k_{rm}r_1) \\ F_{nj}(k_{rm}, r, r_1) &= I_n(k_{rm}r)L_j(k_{rm}r_1) - L_n(k_{rm}r)I_j(k_{rm}r_1) \end{aligned}\right\} \quad (V-4)$$

The Fourier coefficients, b_m, are fixed in terms of a_o through the continuity of E_y, and are

$$b_m = a_o \frac{d}{Y} \frac{C_o(k, r_2, r_3)}{F_o(k_{rm}, r_2, r_1)} \frac{\sin k_{ym} d/2}{k_{ym} d/2} \quad (V-5)$$

Matching the average of the tangential magnetic field B_θ across the slot gives the following transcendental equation for k_{yo} as a function of k:

$$\frac{d}{Y} \sum_{m=-\infty}^{+\infty} \frac{k}{k_{rm}} \frac{C_o(k, r_2, r_3)}{C_{1,o}(k, r_2, r_3)} \frac{F_{1,o}(k_{rm}, r_2, r_1)}{F_o(k_{rm}, r_2, r_1)} \left(\frac{\sin k_{ym} d/2}{k_{ym} d/2}\right)^2 = 1 \quad (V-6)$$

If the dimensions of the line are such that the arguments kr_2, $k_{rm}r_1$, etc., are all small, the various cylinder functions may be replaced by the first term in the expansions about the origin. Further, if k_{yo} is small compared to $\frac{\pi}{Y}$ then only the first term of Eq. (V-6) is important, and $\frac{\sin k_{yo} d/2}{k_{yo} d/2}$ is practically 1. Under these conditions and using the

relation $k_{ro}^2 = k_{yo}^2 - k^2$, Eq. (V-6) reduces to a simple closed form:

$$\frac{R_{yo}}{R} = \frac{\lambda}{\lambda_{yo}} = \sqrt{1 + \frac{d}{Y}\frac{\ln r_2/r_3}{\ln r_1/r_2}} \qquad (V-7)$$

This is to be compared with the corresponding formula for a linear magnetron:

$$\frac{R_{yo}}{R} = \sqrt{1 + \frac{d}{Y}\frac{Ld}{XY}} \quad ,$$

(J. C. Slater, Radiation Laboratory Report V5s, Eq. (Ia:45)).

When r_2 is almost equal to r_3, Eq. (V-7) can be further simplified to:

$$\frac{R_{yo}}{R} = \sqrt{1 + \frac{d}{Y}\frac{r_2 - r_3}{r_3 \ln r_1/r_2}} \qquad (V-8)$$

By expanding C_0 and $C_{1,0}$ in a Taylor series about kr_3 it can be shown that Eq. (V-8) holds even if kr_2 and kr_3 are large provided that $k(r_2 - r_3)$ is small.

Table VII (taken in part from Table I, Radiation Laboratory Report 54-16) compares some measurements made by Professor Harvey and Dr. Lashof, with the values predicted by Eq. (V-7). All measurements were at 9.1 cm. except No. 1 at 10.0 cm.

Table VII

	$2r_1$	$2r_2$	$2r_3$	d	Y	$\frac{\lambda_{yo}}{\lambda}$ (exp)	$\frac{\lambda_{yo}}{\lambda}$ (Eq. V-7)
1	13/10 in.	1/2 in.	3/16 in.	1/8 in.	1/4 in.	.73	.705
2	3/4	1/2	3/16	1/8	1/4	.693	.673
3	13/16	1/2	3/16	1/8	3/8	.785	.773
4	3/4	1/2	3/16	1/8	3/8	.760	.744
5	13/16	1/2	3/16	1/4	3/4	.75	.773
6	13/16	1/2	3/16	1/4	3/8	.68	.653
7	13/16	5/8	3/16	1/8	1/4	.55	.551

On the whole there is good agreement between experiment and theory. (Some later measurements by Dr. Lashof show larger differences but they are questionable due to sagging of the inner conductor.) Fig. 17 indicates how far the approximate Eq. (V-7) may be used. Curve I is a plot of k vs. k_{yo} calculated from Eq. (V-7) for the line denoted as No. 1 in Table VII. Curve II is a similar plot using the more rigorous Eq. (V-6). It is seen that the two agree very closely up to k_{yo} = 1.0 cm.$^{-1}$, k = .75 cm.$^{-1}$ which is just about where the approximations for the cylinder functions break down. Above that point Curve II bends away, reaching a maximum at $k_{yo} = \frac{\pi}{Y} = 4.97$, where k = 2.02. An experimental point at 3.2 cm. agrees fairly well with Curve II.

In calculating the attenuation it is again convenient to divide it into two parts, α_I due to dissipation in the surfaces of outer and inner conductors, and α_{II} due to dissipation in the slot walls. It will be assumed that k_{yo} is small enough that only the first term in the field expansions in Eq. (V-3) need be retained. The average rate of power flow down the line is

$$\overline{S_p} = \frac{2\pi}{2\mu} \int_{r_2}^{r_1} r\, E_r\, B_\theta^* \, dr$$

or

$$\overline{S_p} = \frac{\pi}{\mu} \frac{K^2 K_{yo}}{\omega K_{ro}^2} b_o^2 \int_{r_2}^{r_1} F_{1,o}^2 (K_{ro}, r, r_1)\, r\, dr \qquad (V-9)$$

The integral in Eq. (V-9) can be evaluated[13] in terms of other cylinder functions, and $\overline{S}_p$ is then given by:

$$\overline{S_p} = \frac{\pi}{\mu} \frac{K^2 K_{yo}}{\omega K_{ro}^2} b_o^2 \left\{ \frac{r_1^2}{2} F_{1,o}^2 (K_{ro}, r_1, r_1) - \frac{r_2^2}{2} F_{1,o}^2 (K_{ro}, r_2, r_1) + \frac{r_2^2}{2} F_o (K_{ro}, r_2, r_1) F_{2,o} (K_{ro}, r_2, r_1) \right\} \qquad (V-10)$$

---

(13) See G. N. Watson "Treatise on the Theory of Bessel Functions", Cambridge, 1927, P. 135, Eq. 11, with the transformations z = ix, $F_\mu(x) = e^{-\frac{1}{2}\mu i} C_\mu(x)$

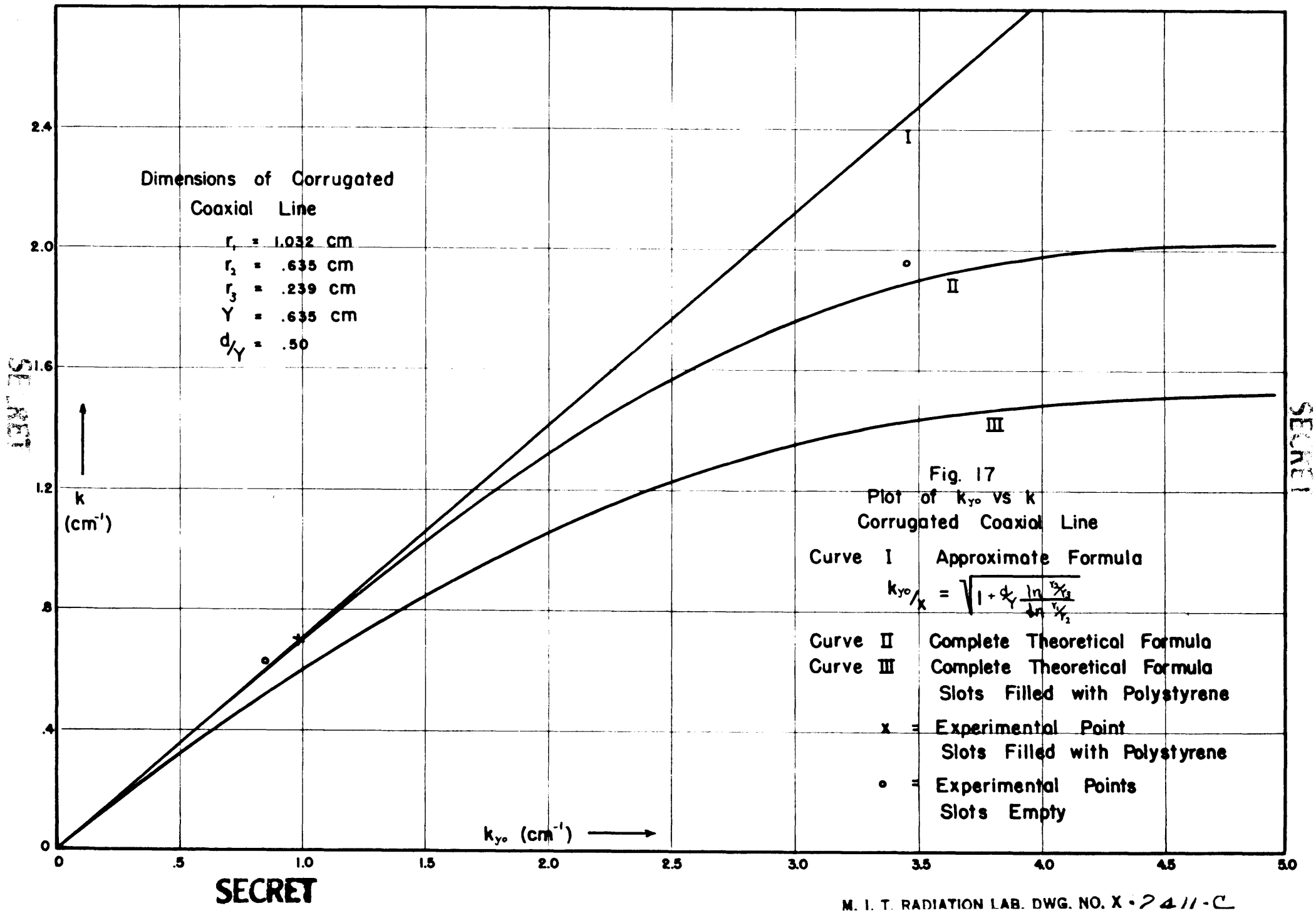

Fig. 17
Plot of k_{yo} vs k
Corrugated Coaxial Line

Curve I Approximate Formula

$$k_{yo}/_{k} = \sqrt{1 + \frac{d}{Y}\frac{\ln \frac{r_3}{r_2}}{\ln \frac{r_1}{r_2}}}$$

Curve II Complete Theoretical Formula
Curve III Complete Theoretical Formula
Slots Filled with Polystyrene

x = Experimental Point
Slots Filled with Polystyrene

o = Experimental Points
Slots Empty

SECRET

SECRET

SECRET

M. I. T. RADIATION LAB. DWG. NO. X-2411-C

The average rate of energy loss in the walls of a slot is found from

$$\overline{S}_d(II) = \frac{1}{2\mu^2}\sqrt{\frac{\mu\omega}{2\sigma}}\int B_\theta^2\, dA$$

where the integral is evaluated over the metal surfaces of the slot. Using the fields given in Eq. (V-1) and evaluating the integrals as in Eq. (V-9) $\overline{S}_d$ (II) turns out to be:

$$\overline{S}_d(II) = \frac{\pi}{\mu^2}\frac{R^2}{\omega^2}\sqrt{\frac{\mu\omega}{2\sigma}}\; a_o^2\left\{r_2^2 C_{1,0}^2(R,r_2,r_3) - r_2^2 C_0(R,r_2,r_3)C_{2,0}(R,r_2,r_3) - r_3(r_3-d)C_{1,0}^2(R,r_3,r_3)\right\} \quad (V-11)$$

The attenuation due to dissipation in the slot is given by:

$$\alpha_{II} = \frac{N}{2}\,\frac{\overline{S}_d(II)}{\overline{S}_P}$$

where N is the number of slots per unit length. From the above equations, and using Eq. (V-5) for b_o in terms of a_o, α_{II} is equal to

$$\alpha_{II} = N\sqrt{\frac{\epsilon\omega}{2\sigma}}\frac{Y^2}{d^3}\frac{R_{ro}^2}{R R_{yo}}\;\frac{r_2^2\dfrac{C_{1,0}^2(R,r_2,r_3)}{C_0^2(R,r_2,r_3)} - r_2^2\dfrac{C_{2,0}(R,r_2,r_3)}{C_0(R,r_2,r_3)} - r_3(r_3-d)\dfrac{C_{1,0}^2(R,r_3,r_3)}{C_0^2(R,r_2,r_3)}}{r_1^2\dfrac{F_{1,0}^2(R_{ro},r_1,r_1)}{F_0^2(R_{ro},r_2,r_1)} - r_2^2\dfrac{F_{1,0}^2(R_{ro},r_2,r_1)}{F_0^2(R_{ro},r_2,r_1)} + r_2^2\dfrac{F_{2,0}(R_{ro},r_2,r_1)}{F_0(R_{ro},r_2,r_1)}}, \quad (V-12)$$

If the arguments of the functions are sufficiently small so that the first term in the expansion about the origin is a good approximation to the function then α_{II} reduces to the simple form:

$$\alpha_{II} = N\sqrt{\frac{\epsilon\omega}{2\sigma}}\;\frac{\lambda_{yo}}{\lambda}\;\frac{\ln r_2/r_3 + d/2r_3}{\ln r_1/r_2} \quad (V-13)$$

where use has been made of the approximate formula Eq. (V-7).

The average rate of energy loss in the walls outside the slot, per slot, is found similarly to be:

$$\overline{S}_d(I) = \frac{\pi}{\mu^2\omega^2}\sqrt{\frac{\mu\omega}{2\sigma}}\;\frac{R^2}{R_{ro}^2}\,b_o^2\left\{r_2 DF_{1,0}^2(R_{ro},r_2,r_1) + r_1 Y F_{1,0}^2(R_{ro},r_1,r_1)\right\}, \quad (V-14)$$

where D is equal to Y-d. The attenuation due to losses in these surfaces is therefore:

$$\alpha_I = N\sqrt{\frac{\epsilon\omega}{2\sigma}}\,\frac{R}{R_{y0}}\,\frac{r_2 D F_{1,0}^2(R_{r0}, r_2, r_1) + r_1 Y F_{1,0}^2(R_{r0}, r_1, r_1)}{r_1^2 F_{1,0}^2(R_{r0}, r_1, r_1) - r_2^2 F_{1,0}^2(R_{r0}, r_2, r_1) + r_2^2 F_0(R_{r0}, r_2, r_1) F_{2,0}(R_{r0}, r_2, r_1)} \qquad (V-15)$$

To the same approximation as (Eq. I-13), α_I can be written as

$$\alpha_I = N\sqrt{\frac{\epsilon\omega}{2\sigma}}\,\frac{\lambda_{y0}}{\lambda}\,\frac{\frac{D}{2r_2} + \frac{Y}{2r_1}}{\ln r_1/r_2} \qquad (V-16)$$

It will be noticed that if r_3 is made equal to r_2, and $D = Y = \frac{1}{N}$, so that the slots vanish, then Eq. (V-16) reduces to the customary formula for attenuation in a coaxial line[14].

The total attenuation of power, expressed in db/m is thus

$$\alpha' = 8.686\, N\sqrt{\frac{\epsilon\omega}{2\sigma}}\,\frac{\lambda_{y0}}{\lambda}\,\frac{\ln r_2/r_3 + d/2r_3 + D/2r_2 + Y/2r_1}{\ln r_1/r_2} \quad db/m. \qquad (V-17)$$

For a brass line of the dimensions given in Fig. 17, α' turns out to be .335 db/m at 9.1 cm., about .26 db/m of this coming from dissipation in the slot walls. No quantitative measurements of the attenuation have yet been made, but Dr. Lashof states that for the line in question it is less than .5 db/m. The theoretical value is therefore quite reasonable.

Case 2. Slots filled with Dielectric

If the slots are filled with a medium of dielectric constant κ Maxwell's equations may be written as

$$\nabla \times E - i\omega B = 0 \qquad \nabla \times B + \frac{i\kappa R^2}{\omega} E = 0$$

$$\nabla \cdot D = 0 \qquad \nabla \cdot B = 0$$

---

[14] J. C. Slater "Microwave Transmission," McGraw Hill, New York, 1942, P.162

Hence in the slots the fields are the same as those in vacuum except that k is replaced everywhere by $k' = \sqrt{K}\,k$, as follows:

$$\left.\begin{aligned} \dot{E}_{yj} &= a_o e^{i k_{yo} j Y} C_o(k', r, r_3) \\ B_{\theta j} &= -\frac{i k'}{\omega} a_o e^{i k_{yo} j Y} C_{1,o}(k', r, r_3) \end{aligned}\right\} \quad (V-18)$$

The fields outside the slots are unchanged of course. The permeability of the medium is the same as that of vacuum, and therefore it is still true that E_y and B_θ must be everywhere continuous. The boundary conditions on the radial component of the electric field are now different, but that component is not included in the matching in any case. The equation for k_{yo} as a function of k is then:

$$\frac{d}{Y}\sum_{-\infty}^{+\infty} \frac{k}{\sqrt{K}\,k_{ym}} \frac{C_o(k', r_2, r_3)}{C_{1,o}(k', r_2, r_3)} \frac{F_{1,o}(k_{rm}, r_2, r_1)}{F_o(k_{rm}, r_2, r_1)} \left(\frac{\sin k_{ym} d/2}{k_{ym} d/2}\right)^2 = 1. \quad (V-19)$$

In the approximate form of this equation, drops out and we are left with Eq. (V-7) again. The dielectric therefore has no influence on the wave length in the line in this approximation, which is true experimentally in many cases.

Table VIII presents some measurements of Dr. Lashof on several lines described in Table VII with the slots filled with polystyrene. Other measurements however seem

Table VIII

Polystyrene-filled Slots

	$\frac{\lambda_{yo}}{\lambda}$ (empty)	$\frac{\lambda_{yo}}{\lambda}$ (polystyrene)	$\frac{\lambda_y}{\lambda}$ (Eq. (IV-7))
1	.73	.698	.705
2	.693	.676	.673
6	.68	.652	.653

to indicate a considerable decrease in the ratio λ_{yo}/λ when k_{yo} becomes large. This is to be expected, since the approximations involved in Eq. (IV-7) should break down at smaller k_{yo} than when the slots are empty. Curve III in Fig. 17 is a plot of k vs. k_{yo} for polystyrene-filled slots as calculated from the more accurate Eq. (V-19). It is asymptotic to Curve I for very small values of k_{yo}, but begins to deviate from it much sooner than the corresponding Curve II for empty slots. It will be noticed however that the experimental point actually lies a good deal higher than Curve III.

The expression for α_{II}, modified by the presence of dielectric (assumed ideal) is given by Eq. (V-12) replacing k in the cylinder functions by k' and multiplying the the fraction by κ. The approximate form of α_{II}, Eq. (V-13), and the attenuation α_I remain unchanged, however. In addition to α_I and α_{II} there is now an attenuation α_{III} due to losses in the volume of the dielectric. These losses may be represented by means of a complex dielectric constant such that the wave number in the dielectric is written in the form:

$$\sqrt{\kappa}\, k = k' + i\, k'' \qquad (V-20)$$

It can then be shown[15] that the average rate of energy loss per unit volume is equal to the real part of $\nabla \cdot S^*$ where $S^* = \frac{1}{2} E \times H^*$. The average rate of dissipation per slot is then

$$\overline{S_d}\,(III) = Re \int \nabla \cdot S^* \, dV = Re \int S^* \cdot n \, dA. \qquad (V-21)$$

For the purposes of calculating α_{III} the metal walls may be considered ideal since the finite conductivity has already been taken into account

---

(15) J. A. Stratton, "Electromagnetic Theory," McGraw Hill, New York, 1941, P. 137

in α_{II}. Eq. (V-21) therefore reduces to an integral over the open face of the slot only. Since k" is very small compared to k', the imaginary parts of the various Bessel and Neumann functions can be accurately calculated from the first term of the Taylor expansion about k'r. Neglecting higher powers of k", $\overline{S}_d$ (III) is therefore:

$$\overline{S}_d(III) = \frac{a_0^2}{2\mu\omega} K' K'' \left\{ r_2 N_0(K' r_3) J_1(K' r_2) - r_3 N_0(K' r_2) J_1(K' r_3) \right\} N_1(K' r_2). \quad (V-22)$$

If the arguments are small enough so that the functions themselves may be represented by the first term in a Maclaurin series the attenuation α_{III} can then be written in the following convenient form:

$$\alpha_m = \sqrt{K}\, N \frac{\delta}{2} \frac{\lambda_{40}}{\lambda} \frac{d}{\lambda} \frac{K^2 r_3^2 N_0(K' r_2) - K^2 r^2 N_0(K' r_3)}{\ln r_1/r_2} \quad (V-23)$$

where is the ratio of the imaginary and real parts of the dielectric constant and is known as the power factor. For a line of the dimensions given in Fig. 17, and using a power factor of .0008 for polystyrene the attenuation α_{III} is .07 db/m in power. There is no available experimental data for α_{III}, but qualitatively the attenuation is of the same order of magnitude as that calculated.

Conclusions:

The formulas and tables presented here enable the resonant modes of vane magnetrons to be computed to an accuracy of 3% or less, and should therefore be of use in the preliminary design of such tubes. The inaccuracy is the result of omitting the cathode, end zones, and field fringing. The latter omission changes the fields considerably but does not affect the results by more than 1%. The cathode likewise may usually be neglected, so that the largest source of error is the effect of the end zones. It has not been possible to calculate this effect except in a qualitative manner. However, the methods used give a clear physical picture of the role of the end zones, and further improvement of the calculation would probably require a disproportionate amount of effort.

The end zones are also of importance in corrugated wave guides. It had been hoped that one could find an end zone size such that the free space wave length is nearly constant for a large variation in guide wave length, corresponding to the mode cross-over found in slot and hole magnetrons. Such a wave guide would be of great importance in linear array antennas since one could then scan by tuning the magnetron slightly. However, it was found that such a cross-over, if it exists, occurs at very small end zone height. Since the attenuation is large for small end zones, this scheme is then not practical. In this connection it might be profitable to investigate corrugated wave guides with a slot and hole arrangement instead of slots, as that form of magnetron has a larger end effect.

Appendix I

Tables of f and G_n

The functions f and G_n are defined as

$$f = \arctan\left\{-\frac{C_{o,1}(R, r_1', r_2')}{C_1(R, r_1', r_2')}\right\} \tag{1}$$

and

$$G_n = \arctan\left\{\sum_{m=n\pm lN} \frac{N\phi}{\pi} \frac{J_m(Rr_1)}{J_m'(Rr_1)} \left(\frac{\sin m\phi}{m\phi}\right)^2\right\} \tag{2}$$

In the range of $x(=k(r_2 - r_1))$ from .8 to 1.2, f can be represented as a linear function of x with an accuracy of .5%:

$$f = aR(r_2 - r_1) + b \tag{3}$$

The coefficients a and b are tabulated as functions of the parameter $y = r_2'/r_1'$ in Table I. Figs. 18 and 19 are graphs of a and b for y between 1.5 and 9.0. G_n can be approximated by a linear function of kr_1:

$$G_n = \alpha_n Rr_1 + \beta_n$$

The coefficients α_n and β_n depend upon n, N, and ϕ. For the range of involved β_n is small and practically constant, while α_n can be considered a linear function of ϕ :

$$\alpha = \gamma_n \phi + \delta_n$$

Table II presents values of γ_n, δ_n and β_n for several values of N. Within the ranges of ϕ and kr_1 stated in the table G_n can be computed to an accuracy of 1%, providing n is greater than 1 or 2, in which case the error is larger, about 5%.

Table I

The Coefficients a and b for Various Values of $y = r_2'/r_1'$

y	a	b
1.5	-1.012	1.438
1.6	-1.000	1.400
1.7	-.986	1.361
1.8	-.977	1.335
1.9	-.965	1.304
2.0	-.951	1.272
2.1	-.937	1.241
2.2	-.925	1.216
2.3	-.910	1.183
2.4	-.895	1.155
2.6	-.873	1.110
2.8	-.846	1.059
3.0	-.820	1.016
3.2	-.798	.975
3.6	-.750	.897
4.0	-.707	.831
4.5	-.658	.759
5.3	-.593	.665
6.0	-.550	.602
7.0	-.495	.530
8.0	-.450	.468
9.0	-.418	.429

Table II

The Coefficients γ_n , δ_n and β_n

		η	γ_n	δ_n	β_n
N 8	$.09 < \phi < .20$	1	2.44	.109	-.011
		2	1.11	.092	-.002
	$.2 < R\gamma_1 < .6$	3	.85	.077	.000
		4	.67	.085	-.001
N 10	$.10 < \phi < .18$	1	2.68	.153	-.009
		2	1.37	.082	-.002
	$.3 < R\gamma_1 < .6$	3	.66	.103	.001
		4	.46	.106	.000
		5	.50	.092	.001
N 12	$.06 < \phi < .12$	1	4.27	.284	-.174
		2	2.15	.057	-.025
	$.8 < R\gamma_1 < 1.2$	3	1.23	.057	-.008
		4	.92	.055	-.003
		5	.67	.060	.002
		6	.57	.066	.001
N 14	$.08 < \phi < .12$	1	4.27	.360	-.256
		2	2.10	.111	-.052
	$.9 < R\gamma_1 < 1.4$	3	1.15	.092	-.024
		4	.88	.064	-.003
		5	.55	.070	.002
		6	.58	.056	.004
		7	.45	.066	.003
N 16	$.04 < \phi < .14$	1	3.41	.413	-.155
		2	2.97	.053	-.030
	$.8 < R\gamma_1 < 1.2$	3	1.61	.046	-.008
		4	1.05	.048	-.005
		5	.68	.052	.002
		6	.58	.049	.001
		7	.52	.047	.000
		8	.44	.049	.002

Table II (continued)

		η	γ_n	δ_n	β_n
N 18	$.04 < \phi < .10$	1	5.10	.350	-.192
		2	2.90	.063	-.028
	$.8 < Kr_1 < 1.2$	3	1.98	.035	-.012
		4	1.27	.044	-.006
		5	.93	.042	.001
		6	.73	.043	.001
		7	.62	.043	.001
		8	.62	.039	-.001
		9	.60	.039	-.001
N 20	$.04 < \phi < .10$	1	5.06	.376	-.172
		2	3.25	.062	-.033
	$.8 < Kr_1 < 1.2$	3	1.90	.048	-.010
		4	1.35	.044	-.005
		5	.92	.046	.001
		6	.73	.045	-.001
		7	.60	.041	.002
		8	.58	.042	.001
		9	.50	.042	.002
		10	.48	.042	.002

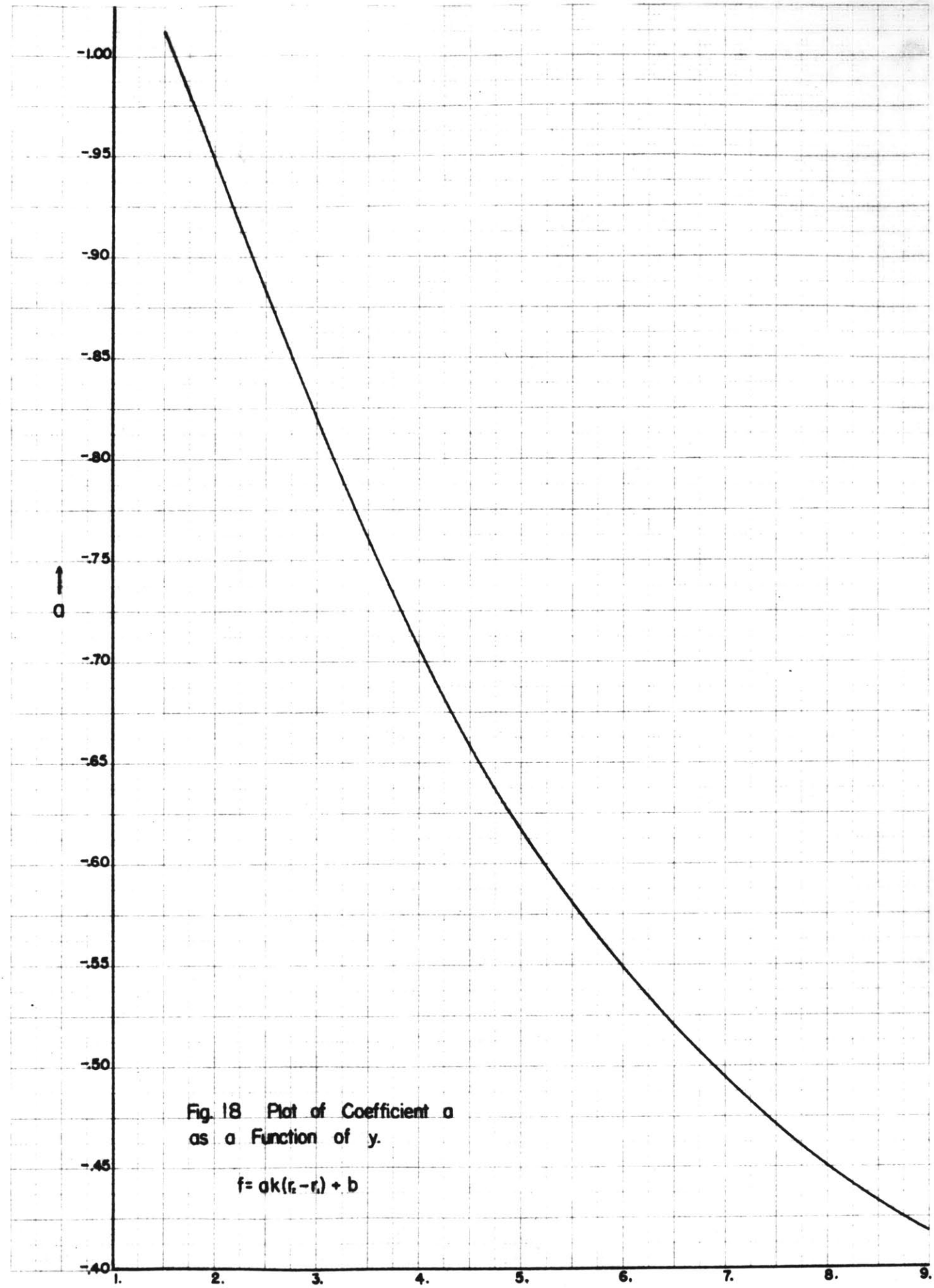

Fig. 18 Plot of Coefficient a as a Function of y.

$f = ak(r_2 - r_1) + b$

NON-RESTRICTED

M. I. T. RADIATION LAB. DWG. NO. X-2385-4

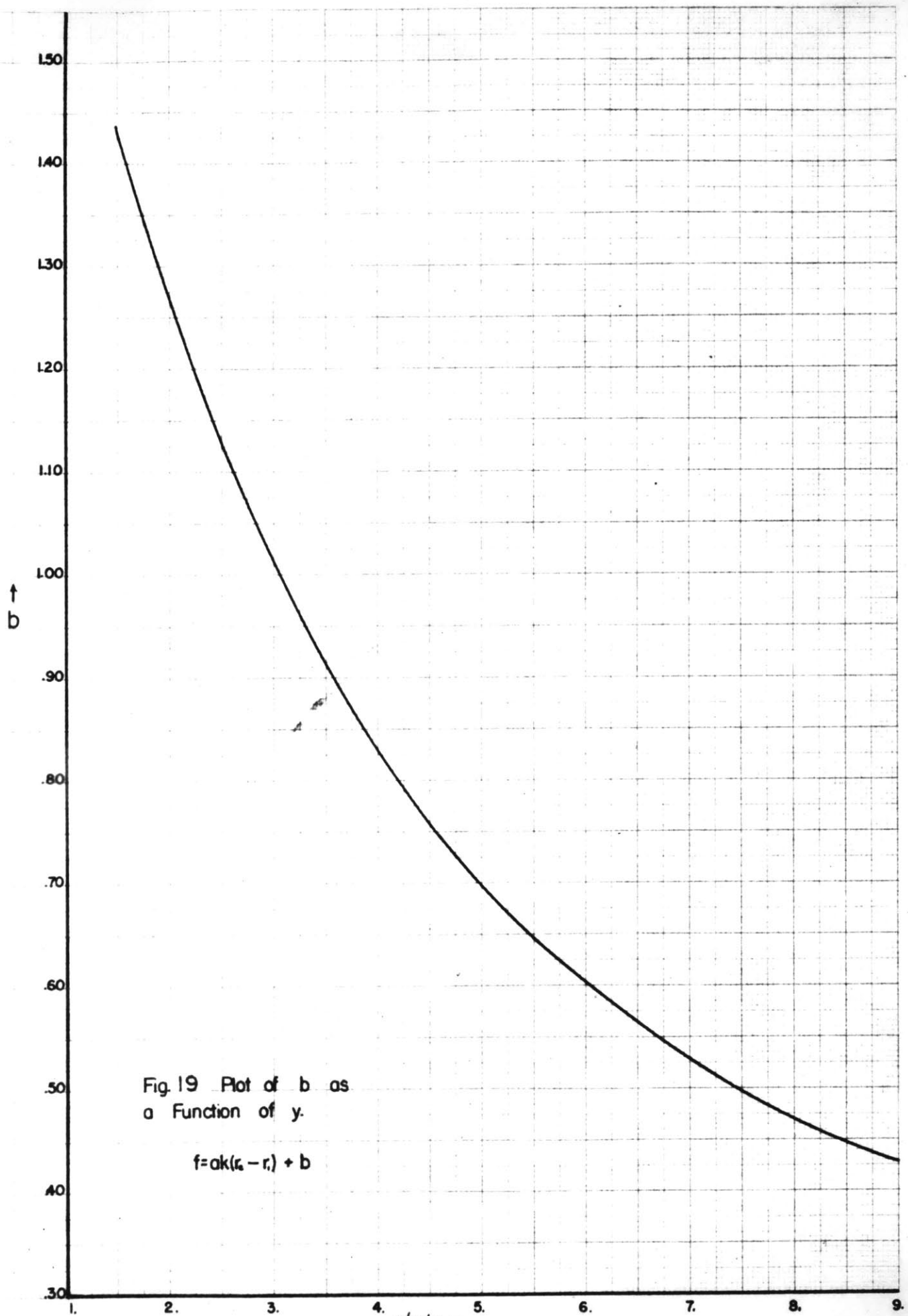

Fig. 19 Plot of b as a Function of y.

$f = ak(r_2 - r_1) + b$

APPENDIX II

Measured Resonant Wave Lengths of a Linear Magnetron

m	Z (centimeters)										
	∞	1.270	0.953	0.699	0.513	0.280	0.064	0.030	0.013	0.000	$z_1 = \infty$
0,2,1		11.700	11.504	11.264	11.030	10.614	9.899	9.715	9.534	9.378	12.642
0,3,1	9.800	9.692	9.631	9.548	9.467	9.264	8.748	8.652	8.334	8.071	9.833
0,4,1	8.912	8.891	8.875	8.837	8.802	8.707	8.354	8.306		7.548	8.912
0,5,1	8.505	8.503	8.491	8.480	8.451	8.401	8.166	8.132		7.298	8.502
0,6,1	8.280	8.286	8.278	8.270	8.262		8.043	8.023		7.156	8.267
0,7,1	8.146	8.148	8.145	8.140	8.134	8.110	7.962			7.063	8.128
0,8,1	8.063	8.069	8.064	8.062	8.057	8.039	7.915			7.004	8.045
0,9,1	8.022	8.026	8.023	8.020	8.017		7.882			6.977	8.004
0,1,2		11.068	10.675	10.195	9.732	9.056	8.016				
0,2,2		9.353	9.159	8.970	8.795	8.464	7.807				
0,3,2	8.438	8.261	8.198	8.144	8.082	7.948	7.602				
0,4,2	7.742	7.707	7.698	7.670	7.654	7.608	7.432				
0,5,2	7.422	7.417	7.412	7.406	7.400	7.384	7.301				
0,6,2	7.249	7.249	7.244	7.245	7.243	7.235	7.210				
0,7,2	7.142	7.147	7.144	7.144	7.133	7.145	7.135				
0,8,2	7.080	7.086	7.082	7.081	7.082	7.080	7.085				
0,9,2	7.049	7.052	7.047	7.047	7.047	7.050	7.053				
0,10,2	7.035	7.034									
0,2,3?		6.907	6.868	6.812	6.761	6.587					

(The column marked $z_1 = \infty$ gives values calculated from Eq. (II-18)).

Appendix III

The Unloaded Q of a Linear Magnetron

The purpose of this calculation is to provide a rough value for the Q due to joulean dissipation for the (0,m,1) modes of a linear magnetron. The following assumptions are made:

1. The end zones are so large that they have little effect on the resonant frequency. Hence B_x in the slots may be neglected. The other field components in the slots are also assumed independent of z.

2. The fields in I and IV are small compared to those in the slots, and hence the energy stored in these regions and the dissipation in the walls may be neglected.

3. The energy of the fields in the end zones is negligible, and the dissipation in the top surfaces of the vanes is much larger than in the other walls of the end zones.

4. Fringing of the field is neglected.

These approximations hold best for the higher modes.

The Q is calculated using the expression[1]:

$$Q = \frac{2}{\delta} \frac{\int B^2 dV}{\int B_t^2 dS} \qquad (1)$$

where B_t is the tangential magnetic field and δ is the skin depth. The components of the fields that will be needed are:

---

[1] J. C. Slater, Radiation Laboratory Report 43-16, P. 43

In the jth slot:

$$\left.\begin{aligned} B_{zj} &= a_0 \cos k_{y0} jY \cos k_x' (x - \bar{X} - L) \\ E_{yj} &= \frac{i\omega}{k_x'} a_0 \cos k_{y0} jY \sin k_x' (x - \bar{X} - L) \end{aligned}\right\} \quad (2)$$

In the end zones

$$\left.\begin{aligned} E_y &= \sum_{\ell=-\infty}^{+\infty} \frac{i\omega}{k_x'} C_\ell \cos k_{y\ell} y \sinh k_{z\ell}'' (z - z_2) \sin k_x' (x - \bar{X} - L) \\ B_y &= \sum_{-\infty}^{+\infty} \frac{k_{y\ell}}{k_{z\ell}''} C_\ell \sin k_{y\ell} y \cosh k_{z\ell}'' (z - z_2) \cos k_x' (x - \bar{X} - L) \end{aligned}\right\} \quad (3)$$

Although standing wave solutions are used here, instead of traveling waves, the relation between c_j and a_o is still given by Eq. (II-21).

The integral of B_z^2 over the volume of the slots is

$$\int B_z^2 \, dV = a_0^2 L z_1 d \left[1 + \frac{\sin 2k_x' L}{2k_x' L} \right] \sum_{j=0}^{N-1} \cos^2 k_{y0} jY$$

$$= \frac{N}{2 - \delta_{mN}} a_0^2 L z_1 d \left[1 + \frac{\sin 2k_x' L}{2k_x' L} \right], \quad (4)$$

where δ_{mN} is the Kronecker symbol.

The integral of B_t^2 over the surfaces of the oscillator cavities is

$$\int_{II} B_t^2 \, dS = \frac{2N}{2 - \delta_{mN}} a_0^2 z_1 \left[d + L \left(1 + \frac{\sin 2k_x' L}{2k_x' L} \right) \right]. \quad (5)$$

The similar integral evaluated over the top surfaces of the vanes is:

$$\int_{III} B_y^2 \, dS = NL \frac{d^2}{Y^2} \sum_{\ell=-\infty}^{+\infty} a_0^2 \frac{k_{y\ell}^2}{k_{z\ell}''^2 \tanh^2 k_{z\ell}'' Z} \left(\frac{\sin k_{y\ell} d/2}{k_{y\ell} d/2} \right)^2 \left[1 + \frac{\sin 2k_x' L}{2k_x' L} \right] \left[D + d\delta_{mN} \frac{\sin k_{y\ell} d}{k_{y\ell} d} \right] \quad (6)$$

where $D = Y - d$.

In calculating the Q, some further simplifications may be made. In the series in Eq. (6) we need keep only the $\ell = 0$ and $\ell = 1$ terms and replace k_z'' by $k_{y\ell}''$. The final value for the Q is then

$$Q = \frac{1}{\delta} \frac{Ld\left[1 + \frac{\sin 2k_x'L}{2k_x'L}\right]}{d + L\left[1 + \frac{\sin 2k_x'L}{2k_x'L}\right] + \frac{2-\delta_{mN}}{2}\frac{L}{\beta_1}\frac{d^2}{Y^2}\left[1 + \frac{\sin 2k_x'L}{2k_x'L}\right]\sum_{\ell=0}^{1}\coth^2 k_{y\ell} Z\left(D + d\delta_{mN}\frac{\sin k_{y\ell} d}{k_{y\ell} d}\right)} \quad (7)$$

BIOGRAPHY

Herbert Goldstein was born on June 26, 1922 in New York City, where he attended elementary and high schools. In September 1936 he entered the College of the City of New York, and was graduated in 1940 with the degree of B. S., Magna Cum Laude, with Honors in Physics. During 1940-41 he was a part-time Tutor at the College of the City of New York, and pursued graduate studies at Columbia University. In 1941 he received an appointment as Teaching Fellow at the Massachusetts Institute of Technology which he held to June 1943. He is a member of Phi Beta Kappa, and an associate of Sigma Xi.